Journal of Medicinal Chemistry

Article

pubs.acs.org/jmc

Synthesis, Biological Evaluation, and Molecular Modeling of Donepezil and *N*-[(5-(Benzyloxy)-1-methyl-1*H*-indol-2-yl)methyl]-*N*-methylprop-2-yn-1-amine Hybrids as New Multipotent Cholinesterase/Monoamine Oxidase Inhibitors for the Treatment of Alzheimer's Disease

Irene Bolea,[†,⊥] Jordi Juárez-Jiménez,[‡,⊥] Cristóbal de los Ríos,[∥] Mourad Chioua,[§] Ramón Pouplana,[‡] F. Javier Luque,[‡] Mercedes Unzeta,*[,†] José Marco-Contelles,*[,§] and Abdelouahid Samadi[§]

[†]Departament de Bioquímica i Biología Molecular, Facultat de Medicina, Institut de Neurociències, Universitat Autònoma de Barcelona, 08193 Bellaterra, Barcelona, Spain

[‡]Departament de Fisicoquímica, Facultat de Farmàcia, and Institut de Biomedicina (IBUB), Universitat de Barcelona, Av. Diagonal 643, E-08028, Barcelona, Spain

[§]Laboratorio de Radicales Libres y Química Computacional (IQOG, CSIC), Juan de la Cierva 3, E-28006, Madrid, Spain

[∥]Instituto Teófilo Hernando, Fundación de Investigación Biomédica, Hospital Universitario de la Princesa, C/Diego de León, 62, E-28029, Madrid, Spain

Supporting Information

ABSTRACT: A new family of multitarget molecules able to interact with acetylcholinesterase (AChE) and butyrylcholinesterase (BuChE), as well as with monoamino oxidase (MAO) A and B, has been synthesized. Novel compounds (**3**–**9**) have been designed using a conjunctive approach that combines the benzylpiperidine moiety of the AChE inhibitor donepezil (**1**) and the indolyl propargylamino moiety of the MAO inhibitor *N*-[(5-benzyloxy-1-methyl-1*H*-indol-2-yl)methyl]-*N*-methylprop-2-yn-1-amine (**2**), connected through an oligomethylene linker. The most promising hybrid (**5**) is a potent inhibitor of both MAO-A (IC_{50} = 5.2 ± 1.1 nM) and MAO-B (IC_{50} = 43 ± 8.0 nM) and is a moderately potent inhibitor of AChE (IC_{50} = 0.35 ± 0.01 μM) and BuChE (IC_{50} = 0.46 ± 0.06 μM). Moreover, molecular modeling and kinetic studies support the dual binding site to AChE, which explains the inhibitory effect exerted on Aβ aggregation. Overall, the results suggest that the new compounds are promising multitarget drug candidates with potential impact for Alzheimer's disease therapy.

A multipotent MAO+ChE inhibitor for Alzheimer's Disease

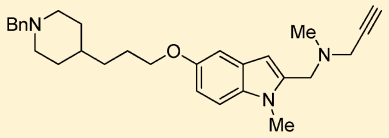

N-((5-(3-(1-benzylpiperidin-4-yl)propoxy)-1-methyl-1*H*-indol-2-yl)methyl)-*N*-methylprop-2-yn-1-amine

IC_{50} (nM) MAO-A	IC_{50} (nM) MAO-B	IC_{50} (μM) EeAChE	IC_{50} (μM) eqBuChE
5.2 ± 1.1	43 ± 8.0	0.35 ± 0.01	0.46 ± 0.06

INTRODUCTION

Alzheimer's disease (AD), the most common form of adult onset dementia, is an age-related neurodegenerative disorder characterized by a progressive memory loss, a decline in language skills, and other cognitive impairments.[1] Although the etiology of AD is not completely known, several factors such as amyloid-β (Aβ)[2] deposits, τ-protein aggregation,[3] oxidative stress,[4,5] and low levels of acetylcholine (ACh) are thought to play significant roles in the pathophysiology of the disease.[6] The selective loss of cholinergic neurons in AD results in a deficit of ACh in specific brain regions that mediate learning and memory functions.[7] However, alterations in other neurotransmitter systems, especially serotoninergic and dopaminergic,[8,9] are also thought to be responsible for the behavioral disturbances observed in patients with AD.[10] This evidence has led to the suggestion that inhibitors of monoamine oxidase (IMAOs) might be also valuable for the treatment of AD.[11,12] Thus, monoamine oxidase (MAO, EC 1.4.3.4), the enzyme that catalyzes the oxidative deamination of a variety of biogenic and xenobiotic amines,[13] is also an important target to be considered for the treatment of specific features of this multifactorial disease. MAO exists as two distinct enzymatic isoforms, MAO-A and MAO-B, based on their substrate and inhibitor specificities.[14] MAO-A preferentially deaminates serotonin, adrenaline, and noradrenaline and is selectively and irreversibly inhibited by clorgyline. In contrast, MAO-B preferentially deaminates β-phenylethylamine and benzylamine and is irreversibly inhibited by *R*-(−)-deprenyl.[15] Selective inhibitors for MAO-A have been shown to be effective antidepressants, whereas MAO-B inhibitors, although apparently devoid of antidepressant action, are useful in the

Received: February 25, 2011
Published: October 24, 2011

 © 2011 American Chemical Society

treatment of Parkinson's disease.[16] Besides the increased amine neurotransmission, the beneficial properties of IMAOs are also related to the reduction of the formation of the neurotoxic products, such as hydrogen peroxide and aldehydes, which promote the formation of reactive oxygen species (ROS) and may ultimately contribute to increased neuronal damage.[17,18] Moreover, AD patients commonly present depressive symptoms that have even been considered as a risk factor for the development of the disease.[19] Increased MAO-B levels due to enhanced astrogliosis in the brain of AD patients have also been reported.[11] Overall, these observations suggest that dual inhibition of MAO-A and MAO-B, rather than MAO-B alone, may be of value for AD therapy.

At present, there are three FDA-approved drugs (donepezil, galanthamine, and rivastigmine)[20−22] that improve AD symptoms by inhibiting acetylcholinesterase (AChE, EC 1.1.1.7), i.e., the enzyme responsible for the hydrolysis of ACh, and thereby raising ACh content in the synaptic cleft. Apart from the beneficial palliative properties of AChE inhibitors in AD,[23−25] cholinergic drugs have shown little efficacy to prevent the progression of the disease. In fact, the multifactorial nature of AD supports the most current innovative therapeutic approach based on the "one molecule, multiple targets" paradigm.[26,27] Thus, a single drug that acts on a specific target to produce the desired clinical effects might not be suitable for the complex nature of AD. Accordingly, the multitarget-directed ligand (MTDL) approach has been the subject of increasing attention by many research groups, which have developed a variety of compounds acting on very diverse targets.[28−33] A very successful approach came from the combination of the carbamate moiety of rivastigmine with the indolamine moiety present in rasagiline, a well-known MAO-B inhibitor, leading to the compound ladostigil.[34] Besides inhibiting MAO and AChE, it possesses neuroprotective and antiapoptotic activities,[35] which have been attributed to the propargylamine group present in the molecule, thus retaining the beneficial properties observed for rasagiline.[36] The potential therapeutic effect of this compound, which has reached clinical trials,[37] is also supported by recent findings showing the ability of propargylamine-containing compounds to modulate cleavage of β-amyloid protein precursor.[38] Hybrid compounds targeting cholinesterases and amyloid plaques,[39] as well as site-activated chelators targeting MAO and AChE, have also been recently attempted.[40−43]

In the development of IMAOs for the treatment of neurodegenerative diseases, our group initially extensively investigated the effect of the introduction of a benzyloxy group in a series of acetylenic and allenic derivatives of tryptamine, which were previously reported to be selective for MAO-A.[44] We observed that the introduction of this moiety changed the selectivity toward the B isoform of the enzyme and that it was significantly decreased when a hydrogen atom was attached to the nitrogen atom of the indole ring and/or the side chain was substituted by a CH_3 group.[45,46] On the basis of these previous works, we have designed a novel family of hybrid compounds of type I to act as potential inhibitors of both MAO and AChE (Figure 1). The novel hybrids have been conceived by a conjuctive approach that combines donepezil (**1**) and *N*-[(5-benzyloxy-1-methyl-1*H*-indol-2-yl)methyl]-*N*-methylprop-2-yn-1-amine (**2**), which is one of the most interesting IMAOs previously investigated in our laboratory.[46] The underlying strategy is to retain the 1-benzylpiperidine fragment present in donepezil (**1**), which binds to the catalytic and mid-gorge sites

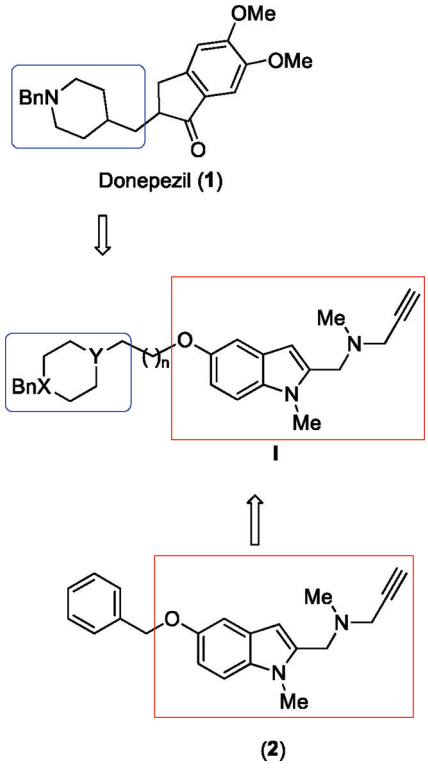

Figure 1. Schematic representation of the conjunctive approach designed to synthesize the novel IMAO/IAChE hybrids.

of AChE, with the 1-methyl-1*H*-indol-2-yl)methyl]-*N*-methylprop-2-yn-1-amine moiety shown in compound **2** (Figure 1), which should occupy the substrate binding site in MAO.

With this conjunctive approach, the novel hybrids are expected to behave as dual binding site AChE inhibitors, since the 1-methyl-1*H*-indol-2-yl)methyl]-*N*-methylprop-2-yn-1-amine moiety could presumably interact at the peripheral anionic site (PAS) of AChE. The possibility of targeting both catalytic active site (CAS) and PAS of AChE will largely depend on the length of the linker, a crucial structural feature to facilitate the binding of both 1-benzylpiperidine and [(1-methyl-1*H*-indol-2-yl)methyl]-*N*-methylprop-2-yn-1-amine moieties to CAS and PAS, respectively, in AChE. This particular mode of action should result in a significant AChE inhibitory potency, of interest for the management of the symptomathology of AD arising from the cholinergic deficit, but more interestingly, it could also recognize the peripheral site, which appears to mediate the Aβ proagreggating action of AChE.[47−50] On the other hand, the correct alignment of the 1-benzylpiperidine and 1-methyl-1*H*-indol-2-yl)methyl]-*N*-methylprop-2-yn-1-amine moieties in MAO will also depend on the tether, as the length and chemical nature of the linker should also affect the accommodation of the hybrid through the residues that define the bottleneck between the entrance and substrate cavities in MAO.

In this work we describe the synthesis, pharmacological evaluation, and molecular modeling of representative molecules of this new family of compounds (**I**, Figure 1). The pharmacological evaluation of these novel compounds includes AChE and butyrylcholinesterase (BuChE) inhibition, the inhibition of MAO-A and MAO-B, the kinetics of enzyme inhibition, and the AChE-dependent and self-induced Aβ aggregation. Finally, molecular modeling studies are performed

to gain insight into the binding mode and structure−activity relationships of the novel hybrid compounds.

RESULTS AND DISCUSSION

Chemistry. To explore the suitability of the conjunctive strategy outline above, compounds **3**−**9** (Figure 2) were

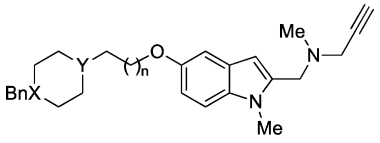

3 X= N, Y= CH, n= 0
4 X= N, Y= CH, n= 1
5 X= N, Y= CH, n= 2
6 X= N, Y= CH, n= 3
7 X= CH, Y= N, n= 1
8 X= CH, Y= N, n= 2
9 X, Y= N, n= 2

Figure 2. General structure for the target molecules **3**−**9**.

synthesized, differing in the length of the tether and the location and/or the number of nitrogens in the tethered-benzyl substituted cyclohexane ring linked to the indolyl moiety.

The 1-benzyl 4-substituted piperidine derivatives **3**−**6** were synthesized by sodium hydride/DMF promoted reaction of compounds **10**−**13** and 1-methyl-2-{[ethyl(prop-2-yn-1-yl)-amino]ethyl}-1*H*-indol-5-ol **14**[51] (Scheme 1).

Scheme 1[a]

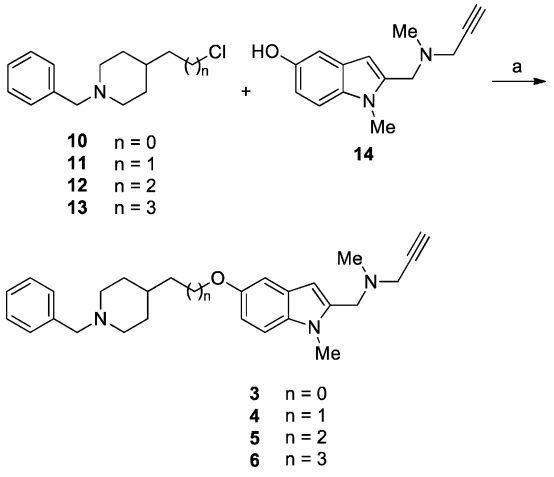

[a]Reagents and conditions: (a) NaH, DMF, room temp.

1-Benzyl-4-(chloromethyl)piperidine **10** and 1-benzyl-4-(chloroethyl)piperidine **11** were synthesized following the methods reported in the literature.[52] 1-Benzyl-4-(3-chloropropyl)piperidine **12** was prepared as shown in Scheme 2, starting from commercial 4-pyridinecarboxaldehyde **15**, via the known intermediate **16**,[53] whose hydrogenation,[54] under Pd/C and PtO_2, in the presence of hydrochloric acid and workup with methanol afforded methyl ester **17**.[55] Next, N-benzylation to give 1-benzylpiperidine **18**, reduction with lithium aluminum hydride (LAH) to provide alcohol **19**,[56] and treatment with thionyl chloride furnished the chloride derivative **12** in quantitative yield.

1-Benzyl-4-(4-chlorobutyl)piperidine **13** was prepared as shown in Scheme 3. Treatment of commercial 1-benzyl-4-

Scheme 2[a]

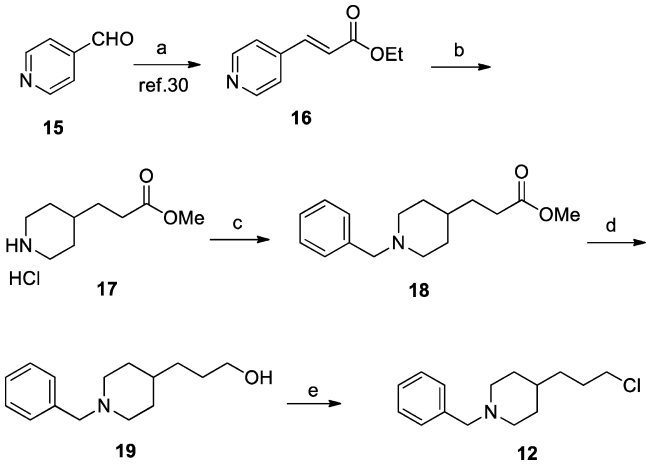

[a]Reagents and conditions: (a) $(EtO)_2P(O)CH_2CO_2Et$, THF, K_2CO_3, reflux (92%); (b) (i) H_2, Pd/C 10%, PtO_2, 4 N HCl in dioxane, EtOH, room temp; (ii) MeOH (90%); (c) BnBr, TEA, CH_2Cl_2 (75%); (d) $LiAlH_4$, THF, reflux (98%); (e) $SOCl_2$, CH_2Cl_2, reflux (99%).

Scheme 3[a]

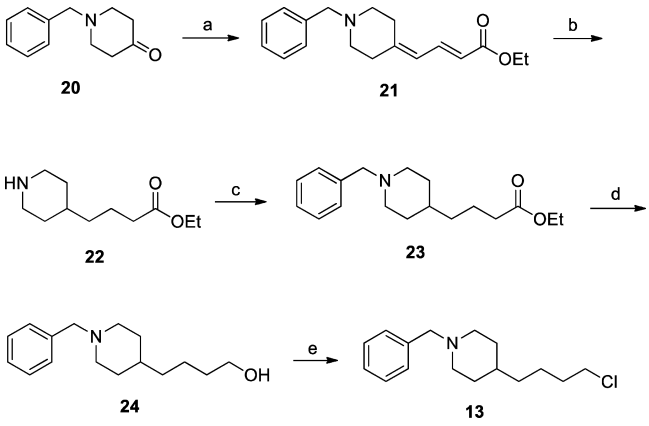

[a]Reagents and conditions: (a) $(EtO)_2P(O)CH_2CH{=}CHCO_2Et$, EtOH, NaH, reflux (78%); (b) H_2, Pd/C 10%, EtOH, room temp (99%); (c) BnBr, TEA, CH_2Cl_2 (70%); (d) $LiAlH_4$, THF, reflux (99%); (e) $SOCl_2$, CH_2Cl_2, reflux (99%).

piperidone **20** with triethyl 4-phosphonocrotonate in the presence of sodium hydride in dry ethanol afforded compound **21** in 78% yield, whose catalytic hydrogenation over Pd/C in ethanol at room temperature gave ester **22** in 99% yield.[57] Next, reaction of **22** with benzyl bromide to give ester **23** followed by reduction with LAH gave the desired alcohol **24**, which was then treated with thionyl chloride to give the chloro derivative **13** in almost quantitative yield.[57]

Compounds **7**−**9** (Figure 2) were synthesized as shown in Schemes 4 and 5. Reaction of indole **14** with 1,2-dibromoethane gave **25**, which after treatment with 4-benzylpiperidine afforded **7** (Scheme 4).[51] Similarly, the reaction of indole **14** with 1,3-dibromopropane gave intermediate **26**, whose reaction with 4-benzylpiperidine or 1-benzylpiperazine afforded **8** and **9**, respectively (Scheme 5).[51]

All new compounds showed analytical and spectroscopic data in good agreement with their structures (see Experimental Part).

dx.doi.org/10.1021/jm200853t | J. Med. Chem. 2011, 54, 8251−8270

Scheme 4[a]

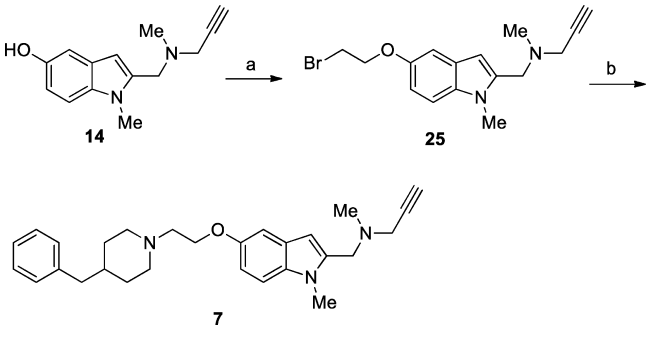

[a]Reagents and conditions: (a) $Br(CH_2)_2Br$, 2-butanone, K_2CO_3, 85 °C, 6 h (37%); (b) 4-benzylpiperidine, $K_2CO_{3)}$ THF, 80 °C (77%).

Scheme 5[a]

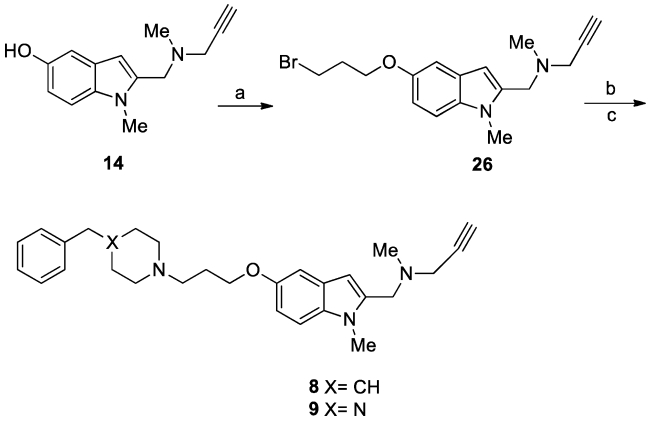

[a]Reagents and conditions: (a) $Br(CH_2)_3Br$, 2-butanone, K_2CO_3, 85 °C, 6 h (80%); (b) 4-benzylpiperidine, K_2CO_3, THF, 80 °C (64%); (c) 1-benzylpiperazine, K_2CO_3, THF, 80 °C (85%).

AChE and BuChE Inhibition. To study the multipotent profile of the hybrid compounds, they were first evaluated as inhibitors of AChE and BuChE. The AChE inhibitory activity was tested against the *Electrophorus electricus* enzyme (*Ee*AChE), and the inhibition of BuChE was carried out using the equine serum enzyme (eqBuChE). The inhibitory activities of the hybrids were compared with those determined for the parent compounds, donepezil (**1**) and *N*-[(5-benzyloxy-1-methyl-1*H*-indol-2-yl)methyl]-*N*-methylprop-2-yn-1-amine (**2**).[46]

Biological Evaluation. The 1-benzylpiperidin-4-yl derivatives **3**–**6** were found to be moderately potent regarding the inhibition of *Ee*AChE. IC_{50} values were similar in all cases (ranging from 0.26 to 0.42 μM, Table 1). Moreover, they exhibit similar potencies against eqBuChE, as IC_{50} values range from 0.46 to 2.1 μM, leading to a very slight selectivity for AChE (the ratio IC_{50}(eqBuChE)/IC_{50}(*Ee*AChE) varies from 1.3 to 5.0). Accordingly, the length of the linker does not seem to be a crucial factor for the inhibitory potency against AChE and BuChE. The most potent compounds are **5** and **6**, which are characterized by IC_{50} values of 0.35 and 0.26 μM against AChE and IC_{50} values of 0.46 and 0.99 μM against BuChE. Compared with donepezil (**1**), they are, respectively, 52- and 39-fold less potent for the inhibition of AChE but 16- and 7-fold more potent regarding the BuChE inhibition.

Compared to derivatives **3**–**6**, reversion of the piperidine ring in **7** and **8** has a dramatic effect on the inhibitory potency in *Ee*AChE. A drastic reduction in activity is also found upon replacement of the piperidine by a piperazine unit (leading to compound **9**). Thus, compounds **7** and **9** are completely inactive against *Ee*AChE, whereas the inhibitory activity of **8** is decreased 52-fold. Nevertheless, these chemical modifications have less effect on the eqBuChE potency, as compounds **7**–**9** are roughly equipotent (**7**) or slightly less potent (**8** and **9**) compared to **3**–**6**.

Table 1. AChE and BuChE Inhibitory Activities of Donepezil (1), the Reference Compound 2, and *N*-[(1-Methyl-1*H*-indol-2-yl)methyl]-*N*-methylprop-2-yn-1-amines 3–9

	IC_{50} (μM)[a]		
compd	*Ee*AChE	eqBuChE	selectivity eqBuChE/*Ee*AChE
1 (donepezil)	0.0067 ± 0.0004	7.4 ± 0.10	1100
2	>100	>100	>100
3 (*n* = 0)	0.31 ± 0.04	1.1 ± 0.20	3.5
4 (*n* = 1)	0.42 ± 0.04	2.1 ± 0.20	5.0
5 (*n* = 2)	0.35 ± 0.01	0.46 ± 0.06	1.3
6 (*n* = 3)	0.26 ± 0.07	0.99 ± 0.08	3.8
7 (*n* = 1)	>100	0.80 ± 0.10	>100
8 (*n* = 2)	18.1 ± 0.40	2.2 ± 0.40	0.12
9 (*n* = 2)	>100	7.6 ± 0.40	>100

[a]Values are expressed as the mean ± standard error of the mean of at least three different experiments in quadruplicate.

Overall, the results point out the relevant role played by the 1-benzylpiperidin-4-yl unit on the AChE inhibitory activity, suggesting that this moiety is the main factor in mediating the binding to AChE. On the other hand, it is worth noting that compounds **3**–**6** are active for the BuChE inhibition. This is particularly important in view of the renewed interest in dual AChE/BuChE cholinergic inhibitors as therapeutic agents for AD, as they have been described to improve cognition.[58] More specifically, compound **5** is presented as a dual ChE inhibitor by having both AChE and BuChE inhibition in the same submicromolar level. For this reason and because of its pharmacological properties, we evaluated its inhibitory activity against human recombinant AChE (hrAChE), the cerebral enzyme expressed in the HEK-293 cell line, and human serum BuChE (hBuChE). Thus, compound **5** inhibited hrAChE with an IC_{50} of 0.38 ± 0.05 μM (tacrine, used as a standard, inhibited hrAChE with an IC_{50} of 122 ± 2 nM) and hBuChE with an IC_{50} of 1.7 ± 0.2 μM (tacrine inhibited hBuChE with an IC_{50} of 36 ± 4 nM).

Kinetic Studies. To gain further insight into the mechanism of action of this family of compounds on AChE, a kinetic study was carried out with the most promising compound of the series, **5**, using *Ee*AChE. Graphical analysis of the reciprocal Lineweaver–Burk plots (Figure 3) showed both increased slopes (decreased V_{max}) and intercepts (higher K_m) at increasing concentration of the inhibitor. This pattern indicates a mixed-type inhibition and therefore supports the dual site binding of this compound. Replots of the slope versus concentration of compound **5** gave an estimate of the inhibition constant, K_i, of 149 nM.

MAO Inhibition. To complete the study of the multipotent biological profile of the hybrid compounds, the inhibitory activity against MAO-A and MAO-B (from rat liver mitochondria) was determined and compared with the inhibition exerted by the parent compounds donepezil (**1**)

dx.doi.org/10.1021/jm200853t | *J. Med. Chem.* 2011, 54, 8251–8270

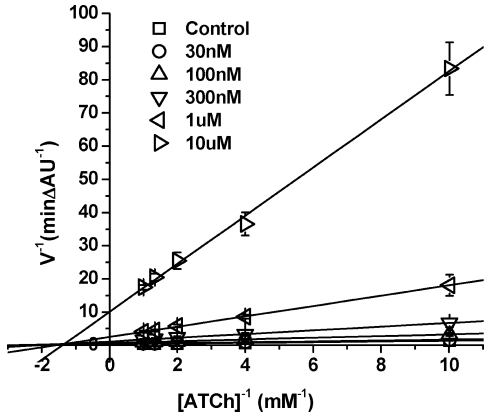

Figure 3. Kinetic study on the mechanism of *Ee*AChE inhibition by compound **5**. Overlaid Lineweaver–Burk reciprocal plots of AChE initial velocity at increasing substrate concentration (0.1–1 mM) in the absence of inhibitor and in the presence of **5** are shown. Lines were derived from a weighted least-squares analysis of the data points.

and *N*-[(5-benzyloxy-1-methyl-1*H*-indol-2-yl)methyl]-*N*-methylprop-2-yn-1-amine (**2**).

Biological Evaluation. The 1-benzylpiperidin-4-yl derivatives **3**–**6** showed a potent MAO-A inhibition (Table 2), acting

Table 2. MAO-A and MAO-B Inhibitory Activities of Donepezil (1), Reference Compound 2, and the *N*-[(1-Methyl-1*H*-indol-2-yl)methyl]-*N*-methylprop-2-yn-1-amine Derivatives (3–9)

	IC_{50} (nM)[a]		
compd	MAO-A	MAO-B	selectivity MAO-B/MAO-A
1 (donepezil)	850000 ± 13000	15000 ± 2200	0.020
2	100 ± 7.0	63 ± 2.0	0.63
3 (n = 0)	82 ± 3.0	750 ± 20	9.1
4 (n = 1)	6.7 ± 1.8	130 ± 41	19
5 (n = 2)	5.2 ± 1.1	43 ± 8.0	8.3
6 (n = 3)	10 ± 4.0	2700 ± 110	260
7 (n = 1)	140 ± 44	1400 ± 500	10
8 (n = 2)	65 ± 17	11000 ± 2400	170
9 (n = 2)	31 ± 14	1600 ± 710	54

[a]Values are expressed as the mean ± standard error of the mean of at least three different experiments in quadruplicate.

in the nanomolar range (IC_{50} ranging from 82 ± 3.0 to 5.2 ± 1.1 nM). In contrast, they were less potent against MAO-B, with the exception of **5**, which was found to be the most potent compound toward both isoforms (IC_{50} of 5.2 ± 1.1 and 43 ± 8.0 nM for MAO-A and MAO-B, respectively). The most selective inhibitor was compound **6** (n = 3) toward MAO-A, whereas **5** was much less selective. It is worth noting the large sensitivity of the inhibitory potency on the length of the tether. Thus, removal of a single methylene group in **6** to yield **5** increased the inhibitory potency against MAO-A and MAO-B by a factor of 2 and 63, respectively. Likewise, further reduction of the tether to just one methylene (from **5** to yield **4**) did not affect the MAO-A inhibitory potency but reduced the potency against MAO-B by 3-fold.

Compounds **7** and **8**, bearing a 4-benzylpiperidin-1-yl residue, also inhibited MAO-A quite potently but showed less potency toward MAO-B. Similarly, compound **9**, containing a 4-benzylpiperazin-1-yl residue, also showed a good MAO-A inhibitory potency but a lower activity toward MAO-B. Interestingly, we found that compound **7** was 21-fold and 11-fold less potent for MAO-A and MAO-B, respectively, than the analogous inhibitor **4**. Similarly, compounds **8** and **9** were significantly less potent for both isoforms than the analogous inhibitor **5** (12-fold and 6-fold for MAO-A and 256-fold and 38-fold for MAO-B, respectively). Altogether, these results show that compounds bearing the donepezil 1-benzylpiperidin-4-yl motif were the best MAO inhibitors and that, among them, **5** was the most potent inhibitor, even more than the reference compound **2**.

Kinetic Studies. To study the type of inhibition toward MAO, we analyzed the reversibility/irreversibility of the binding of compound **5**, the most potent inhibitor of the series. We observed that **5** irreversibly inhibited MAO-A, since the inhibition was not reverted after three consecutive centrifugations and washings with buffer (Figure 4A). This hypothesis is also in agreement with the time-dependent inhibition of MAO-A upon incubation with the inhibitor (Figure 4B) and thus reflects the inhibition mechanism found for the parent compound **2**.[46] Strikingly, whereas the inhibition of MAO-B was also found to depend on the incubation time (Figure 4D), a significant fraction (80.5 ± 3.3%) of the activity was recovered by washing the enzyme three times after incubation for 30 min (Figure 4C). These findings point out that the addition of the benzylpiperidine unit to the reference compound **2** in order to yield **5** does not affect the proper alignment of the indolylpropargylamino moiety in the binding cavity of MAO-A, thus leading to the complete inactivation of the enzyme by chemical modification of the cofactor. However, the present results suggest that docking of **5** into the binding cavity of MAO-B is more impeded than in MAO-A, which should prevent the proper alignment of the propargylamino moiety, thus making less efficient the inactivation of the enzyme.

To clarify the different behavior of **5** toward MAO-A and MAO-B, we further investigated the progress curves of substrate consumption for a longer period in the presence of the inhibitor. As expected, the final rate became zero in both cases, proving that the inhibition of **5** toward both MAO-A and MAO-B occurs in an irreversible process. Nevertheless, the time needed for the total inactivation of MAO-B was higher than that needed for MAO-A (Figure 5), thus showing that although irreversible, the inactivation of MAO-B by **5** is clearly slower. These findings explain the different behavior found in the reversibility studies, which were performed preincubating the enzymes with **5** for 30 min. Figure 5 shows that at this time the velocity of the reaction for MAO-A was clearly decreased and thus substrate consumption was rapidly approaching zero. In contrast, the velocity of the reaction for MAO-B shows a little reduction at 30 min preincubation time, thus supporting the suggestion that docking of **5** into the cavity of MAO-B is more impeded than in MAO-A, resulting in a slower substrate consumption and explaining the recovery of MAO-B activity in the reversibility study.

The kinetic behavior of **5** toward MAO-B determined from the initial rates showed that this compound behaves as a noncompetitive inhibitor, as shown in the Lineweaver–Burk plot (Figure 6A). Thus, the V_{max} decreased as the amount of **5** was increased, whereas the K_M value remained constant (Figure 6B). Determination of Michaelis constants gave a value of K_M = 6.7 ± 0.3 μM and V_{max} = 277.8 ± 6.1 pmol/min for MAO-B

dx.doi.org/10.1021/jm200853t | *J. Med. Chem.* 2011, 54, 8251–8270

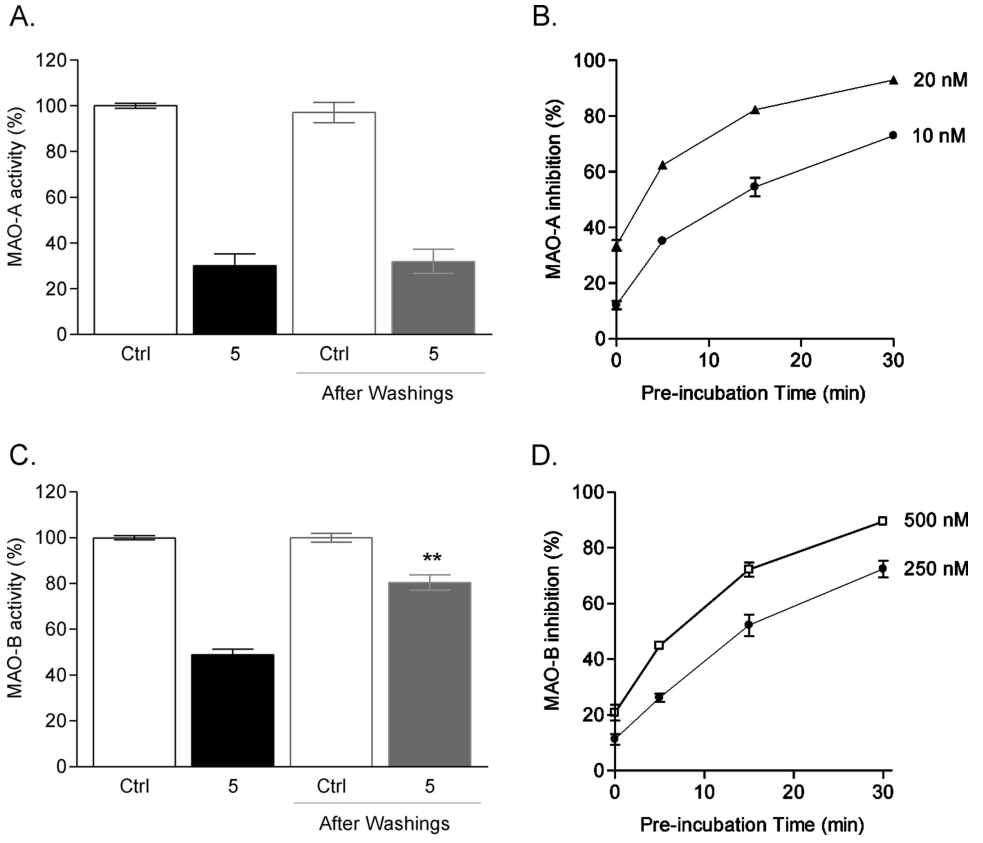

Figure 4. Reversibility studies of MAO-A and MAO-B inhibition by compound **5**. MAO-A (A) and MAO-B (C) were inhibited at 6 and 45 nM **5**, respectively, for 30 min. Then three consecutive washings were performed with buffer. MAO-B inhibition (C) was reverted (recovering 80.5 ± 3.3% of enzyme activity), whereas the inhibition of MAO-A remained unaltered after washings (A). Time-dependence inhibition was studied at several times of preincubation (0−30 min) of MAO with compound **5**. Both MAO-A (B) and MAO-B (D) inhibition were found to be time-dependent. Data are the mean ± SEM of four independent experiments in triplicate.

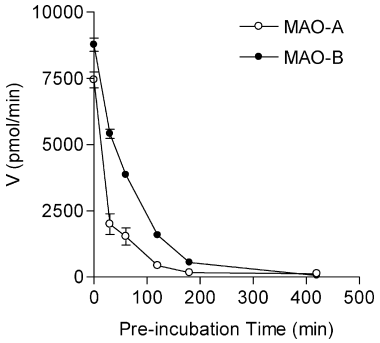

Figure 5. Progress curves of substrate consumption for MAO-A (5-HT, 100 μM) and MAO-B (PEA, 20 μM) in the presence of **5** (10 nM for MAO-A and 100 nM for MAO-B). MAO-A and MAO-B were preincubated with the inhibitor for a long period (0−420 min), and the catalytic activity was determined. The time needed for the total inactivation of the enzyme was greater for MAO-B than for MAO-A. Data are the mean ± SEM of three independent experiments in triplicate.

substrate, β-phenylethylamine (PEA), and an estimated K_i of 11.0 ± 0.39 nM.

Molecular Modeling. The preceding studies point out that **5** seems to be a promising multitarget inhibitor. However, they also show distinctive trends in the pharmacological profile. First, it is unclear why the inhibitory potency against AChE (and BuChE) is slightly affected by the length of the tether, whereas it has a large effect in the inhibition of both MAO-A and MAO-B. Moreover, reversion of the piperidine unit in compounds **5** and **8** notably affects the inhibition of both AChE and MAO. Finally, **5** leads to an irreversible inhibition of MAO-A, whereas inactivation of MAO-B is slower. To shed light onto these questions, a series of docking and molecular dynamics (MD) simulations were conducted to identify the binding mode of **5** to AChE, BuChE, MAO-A, and MAO-B.

AChE Inhibition. The binding mode of **5** to AChE was investigated by considering three structural models of the enzyme, which were built up taking advantage of the X-ray structure of donepezil bound to *Torpedo californica* AChE (*Tc*AChE, PDB entry 1EVE).[59] These models retain the structural details of the benzylpiperidine moiety bound to the AChE gorge but differ in the orientation of Trp279 (numbering in *Tc*AChE), as the inspection of the available X-ray structures for complexes of AChE with dual site binding inhibitors reveals that Trp279 adopts three main conformations at the PAS.[60,61] Thus, the side chain of Trp279 can be characterized by dihedral angles χ_1 (N−C_α−C_β−C_γ) and χ_2 (C_α−C_β−C_γ−$C_{\delta 2}$) close to (i) −60° and −80°, (ii) −120° and +50°, and (iii) −160° and −120°. Representative structures of these orientations are PDB entries 1EVE, 2CKM, and 1Q83, which correspond to the AChE complexes with donepezil, bis(7)-tacrine,[62] and *syn*-TZ2PA6,[63] respectively. In the following these models will be denoted AChE(1EVE), AChE(2CKM) and AChE(1Q83).

The binding of **5** to the three AChE models was first explored by docking calculations performed with rDock,[64,65] which yielded reliable predictions for the binding mode of

dx.doi.org/10.1021/jm200853t | *J. Med. Chem.* 2011, 54, 8251−8270

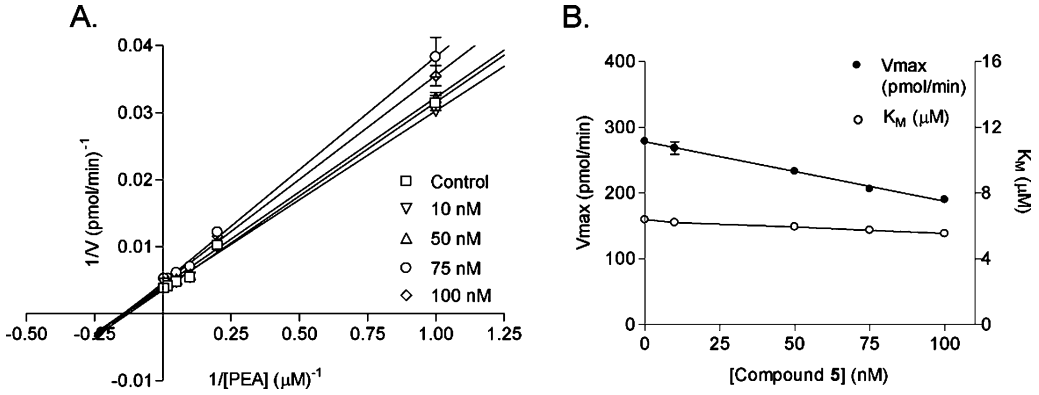

Figure 6. Kinetic study on the mechanism of MAO-B inhibition by **5**. (A) Overlaid Lineweaver–Burk reciprocal plots of MAO-B initial velocity at increasing substrate concentration (PEA, 1–200 μM) in the absence or presence of **5** (10–100 nM) are shown. Lines were derived from a weighted least-squares analysis of the data points. (B) V_{max} decreased as the amount of **5** increased, whereas the K_M value remained constant. Data are the mean ± SEM of four independent experiments in triplicate.

known dual site binding AChE inhibitors.[60] Suitable restraints were introduced to impose the benzylpiperidine moiety to mimic the known binding mode of the same fragment of donepezil in its complex with *Tc*AChE.[59] In turn, this permits enhancement of the conformational sampling of the indolylpropargylamino moiety at the PAS. Finally, the structural integrity and energetic stability of the binding mode proposed for each AChE–**5** complex were examined from the snapshots sampled in 20 ns MD simulations. For the sake of comparison, an additional 20 ns MD simulation was run for the complex between AChE and donepezil.

MD simulations yielded stable trajectories in the last 10 ns, as noted by the time evolution of the potential energy and the root-mean-square deviation (rmsd) of the protein backbone, which ranged from 1.4 to 1.6 Å (a rmsd value of 1.3 Å was obtained for the AChE–donepezil complex; see Figures S1 and S2 in Supporting Information). The rmsd values of the residues that delineate the binding site in catalytic, mid-gorge, and peripheral sites (defined as those residues with at least one atom placed at a distance less than 4 Å from the ligand) were stable for AChE–donepezil (1.4 Å) and AChE(1EVE)–**5** (1.6 Å) complexes, they being similar to the rmsd values determined for the backbone. Larger rmsd values were found for the binding site residues in AChE(2CKM) (2.0 Å) and AChE-(1Q83) (1.7 Å).

No large structural alterations were found in the catalytic site, and the benzylpiperidine moiety adopts a similar arrangement in all cases (Figure 7). Little structural fluctuations were also found in the mid-gorge and peripheral sites for complexes AChE–donepezil and AChE(1EVE)–**5**. In particular, the indanone unit of donepezil and the indolyl ring of **5** were stacked against Trp279, whose side chain was stable along the trajectory. Thus, the torsional angles χ_1 and χ_2 showed small fluctuations around average values of −70° and −110° (see Figure S3 in Supporting Information; the corresponding angles in 1EVE are −52° and −84°). In contrast, larger rearrangements were found at the PAS, mainly involving Trp279, for AChE(1Q83)–**5** and AChE(2CKM)–**5**. In the former case χ_1, which was initially assigned a value close to 180° (as found in 1Q83), remained stable during the first 11 ns but then suddenly changed to a value close to −60° (see Figure S3). Thus, the initial binding mode, which was chosen to mimic the orientation of *syn*-TZ2PA6 bound to *Tc*AChE, was lost and Trp279 adopted a new arrangement close to the conformation

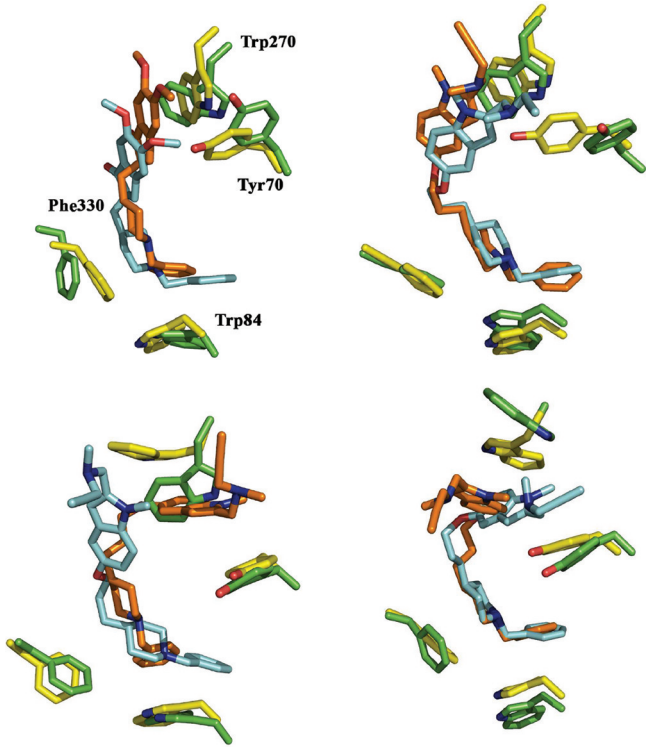

Figure 7. Representation of the binding mode of donepezil and **5** at the beginning and end of the MD simulations: (top left) AChE–donepezil (started from the X-ray structure in PDB entry 1EVE); (top right) AChE(1EVE)–**5**; (bottom left) AChE(1Q83)–**5**; (bottom-right) AChE(2CKM)–**5**. Relevant residues at the catalytic (Trp84, Phe330) and peripheral (Trp279, Tyr70) binding sites are also shown. The ligand/residues at the end of the simulations are shown in blue/green, respectively (the representation at the beginning of the simulation is made in orange/yellow).

found in the AChE–donepezil and AChE(1EVE)–**5** complexes (see above and Figure 7). With regard to AChE(2CKM)–**5**, Trp279 was initially oriented to reproduce the conformation found in the *Tc*AChE–bis(7)-tacrine complex (characterized by χ_1 and χ_2 close to −120° and +50°). After 3 ns, the angle χ_1 changed to 180° and remained stable for 3 ns but then changed to a new value of +60°, which was stable along the rest of the trajectory (see Figure S3 in Supporting Information). Such a change was accompanied by the readjustment of χ_2, which

dx.doi.org/10.1021/jm200853t | *J. Med. Chem.* 2011, 54, 8251–8270

adopted a value close to +90°. At the end of the simulation, a novel structure was obtained where the protonated propargylamino unit remains close to Tyr70 but has lost the interactions with Trp279 (see Figure 7).

The preceding analysis demonstrates the structural integrity of the AChE(1EVE)−**5** model, which mimics the structural features of the binding of donepezil to *Tc*AChE. The reliability of this binding mode is reinforced by the conformational change observed in the PAS of the AChE(1Q83)−**5** complex, which leads to a binding mode close to that found in AChE(1EVE)−**5**, and by the structural change found in AChE(2CKM)−**5**, which leads to a binding mode characterized by a conformation of Trp279 that, to the best of our knowledge, has no counterpart in the available X-ray structures of AChE complexes deposited in the PDB. As a further test, we have determined the relative binding affinity between models AChE(1EVE)−**5** and AChE(2CKM)−**5** by means of MM/PBSA calculations. They were performed for 100 snapshots taken evenly during the last 5 ns of the trajectories using both the standard radii implemented in the AMBER force field and an alternative set of atomic radii that have been explicitly optimized for their use in MM/PBSA calculations with AMBER.[66] The results (see Table S1 in Supporting Information) indicate that binding of **5** to AChE(1EVE) is favored by near 2.3 (standard radii) and 4.0 (optimized radii) kcal/mol relative to AChE(2CKM). Similar trends were observed when MM/PBSA computations were performed by retaining a single water molecule that was hydrogen-bonded to the protonated nitrogen of the piperidine unit of the ligand along the trajectories (data not shown).

The preceding structural and energetic analysis suggests that compound **5** mimics the binding mode of donepezil (see Figure S4). Thus, the benzylpiperidine moieties of donepezil and **5** exhibit a similar alignment in the CAS, though there is a weaker overlap between the benzene unit of **5** and the indole ring of Trp84. More importantly, there is a change in the orientation of residues Tyr334 and Asp72, which remain hydrogen-bonded but are displaced toward the PAS. In turn, this structural change facilitates the stacking of the indole ring of **5** between the aromatic rings of Tyr334 and Trp279. On the other hand, there is a water molecule that bridges the protonated nitrogen of the piperidine unit with the hydroxyl groups of Tyr121 and Ser122 (not shown in Figure 8 for the sake of clarity). Finally, the largest structural flexibility of the inhibitor is localized in the propargylamino unit, which forms transient van der Waals interactions with the benzene ring of Tyr70.

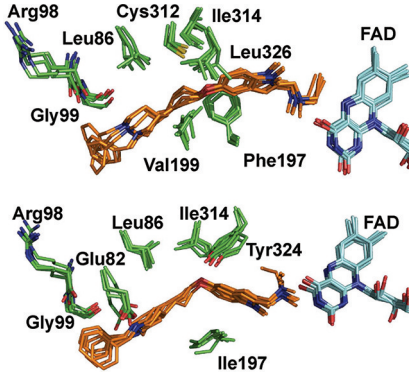

Figure 8. Representation of the binding mode of **5** in (top) MAO-A and (bottom) MAO-B. Five snapshots taken every ns along the last 5 ns of the trajectory are superposed. The ligand is shown as orange sticks, FAD as blue sticks, and selected residues in the entrance and substrate cavities as green sticks.

This binding mode allows us to rationalize the low sensitivity of the inhibitory activity on the length of the tether, as (i) it is reasonable to expect that the benzylpiperidine moiety will fill the same binding pocket but (ii) shortening or lengthening of the tether will be accompanied by displacements of the indole ring of **5** along the gorge that would retain the stacking against Tyr334 or Trp279 (see Figure S5 in Supporting Information). On the other, the lower inhibitory potency associated with reversion of the piperidine unit (compounds **5** and **8**) can be explained by two factors: (i) the lost of the water-assisted hydrogen bonds formed between the protonated nitrogen and Tyr121 and Ser122 (data not shown) and (ii) the weakening of the electrostatic stabilization due to cation−π interactions with the aromatic rings of Phe330 and Trp84 and with the negative charges of Asp72 and Glu198 (see Figure S6).

As a final test, we explored the suitability of an alternative binding mode where the orientation of **5** was reverted so that the propargylamino group fills the CAS and the benzylpiperidine moiety occupies the PAS. As in the preceding discussion, compound **5** was docked in the binding site of the enzyme for the three AChE structural models (1EVE, 1Q83, and 2CKM) but without imposing positional restraints. Inspection of the first ranked poses showed a preference for the placement of the benzylpiperidine moiety in the CAS. Thus, only 1, 7, and 2 poses out of the first 13, 15, and 7 ranked solutions (covering a range of 8 kcal/mol in the score in each case) corresponded to the reverted orientation of **5** upon docking to models AChE_1EVE, AChE_1Q83 and AChE_2CKM, respectively, which reinforces the reliability of the binding mode discussed above. To further explore the suitability of the inverted binding mode, a series of 20 ns MD simulations were run for the three AChE complexes with the reversed orientation of the inhibitor. Inspection of the binding mode sampled along the last 10 ns of the trajectory run for AChE_1EVE (Figure S7) shows that the propargylamino unit remains stacked onto the indole ring of Trp84, filling part of the region occupied by the benzyl moiety of donepezil. However, there are notable structural fluctuations of the methylated indole ring of **5**, which eventually leads to steric clashes with the benzene ring of Phe330. Similarly, the large fluctuations of the benzylpiperidine moiety also argue against a firm stacking with Trp279 at the PAS. The structural instability of the ligand was also found in the simulations run for AChE_1Q83 and AChE_2CKM (see Figure S7), particularly seen in the large mobility of the ligand at the PAS, which affects the stacking between Trp279 and Tyr70. In fact, comparison of the relative free energies determined from MM/PBSA calculations for the different AChE complexes also supports the energetic destabilization of the inverted binding mode (see Table S2). Finally, let us remark that the enhanced flexibility of the piperidine moiety in the PAS, which reflects the lack of strong interactions, does not provide a straightforward explanation to the significant reduction in the inhibitory potency found upon reversion of the ring (compare **5** and **8** in Table 1).

BuChE Inhibition. The binding mode of **5** to BuChE was explored by means of docking calculations (see Experimental Part). The results indicate a marked preference for the insertion of the benzylpiperidine moiety in the CAS, as noted by the fact that only 4 out of the first 20 ranked poses (comprising a range of 5 kcal/mol in the score) were found with the inverted

arrangement (in fact, the first inverted pose was ranked as the ninth solution). Hence, a new docking calculation was run imposing the benzene unit of **5** to stack against Trp79 (equivalent to Trp84 in the CAS of AChE), thus mimicking the interaction found in the AChE complex with donepezil (PDB entry 1EVE). Even in this case, the results indicate a substantial degree of flexibility to accommodate **5** in the binding site of BuChE, especially regarding the indolylpropargylamine moiety but also even the piperidine ring (see Figure S8). Nevertheless, this finding is not unexpected because of the wider volume of the binding site in BuChE compared to AChE, which can be ascribed to mutations between specific binding site residues in the two enzymes, such as the replacement of Phe330 in the CAS of AChE by Ala, the substitution of Tyr70 and Phe290 at the mid-gorge of AChE by Asn and Val, respectively, and the mutation of Trp279 in the PAS of AChE by Ala. Accordingly, it can be expected that the binding of **5** to BuChE will be mainly guided by the interactions due to the benzylpiperidine moiety, thus explaining the lack of large differences in the selectivity between the two enzymes.

MAO Inhibition. The binding mode of hybrid **5** in MAO-A and MAO-B was investigated in order to explain the different inhibitory behavior found for the two isoforms. To this end, we first explored the potential binding mode of **5** by means of docking calculations, which showed a clear preference to accommodate the indolylpropargylamino unit in the substrate cavity. In fact, this is not surprising, as the reference compound **2** was found to be an irreversible inhibitor of the two MAO isoforms, which indicates that the binding mode places the propargylamino unit properly oriented to react with the flavin adenine dinucleotide (FAD) present in the substrate cavity of both MAO-A and MAO-B.[43] Then a representative member of the most populated cluster of the docked poses was chosen as starting structure for MD simulations of the complexes of **5** with MAO-A and MAO-B. In the two cases MD simulations yielded stable trajectories, as noted by inspection of the time evolution of the potential energy and by the small fluctuations of the rmsd profile along the last 5 ns of the trajectories (see Figures S9 and S10). Thus, the rmsd determined for the protein backbone in the MD simulations run for MAO-A and MAO-B is close to 1.4 Å, whereas the rmsd determined for the residues that define the walls of the binding cavity amounts to 2.0 Å.

Inspection of Figure 8 clearly shows that binding of **5** to MAO-A has little effect on the residues that delineate the binding site, suggesting a suitable fit of the indolylpropargylamino unit in the substrate cavity. In fact, the indole fragment of **5** matches well the corresponding moiety in harmine, as noted upon superposition of the X-ray structure of the human MAO-A–harmine complex[67] and the last snapshot of the MD simulation (see Figure S11). The only exception to the structural integrity of the binding pocket concerns few residues located at the entrance of the gorge leading to the substrate cavity, which reflects the adjustment of the ligand, as expected from the larger flexibility of the solvent-exposed loops that shape the entrance cavity (see Figure S11). It is worth noting how the tether fills the hydrophobic region that defines the bottleneck of the binding pocket, which is mainly due to Phe208 and Ile325. The dependence of the inhibitory potency with the length of the tether can be explained by the steric contraints imposed by the side chains of vicinal apolar residues, such as Leu97, Leu337, Val210, and Cys323, as shortening of the tether would lead to steric clashes with the piperidine unit of the ligand. On the other hand, simulations also show that the positive charge of the piperidine unit in **5** is stabilized by water-mediated hydrogen bond interactions with the backbone carbonyl groups of Arg109 and Gly110.

The structural integrity of the binding mode of **5** in MAO-B is also supported by inspection of the snapshots collected at the end of the trajectory (Figure 8). The five-membered ring of the indole moiety of **5** superposes the benzene ring of deprenyl in its complex with human MAO-B (PDB entry 2BYB;[67] see Figure S12). As in MAO-A, the tether occupies the hydrophobic region delineated by residues Ile199, Ile316, Tyr326, and Leu88, which presumably would lead to steric clases with the piperidine ring upon shortening of the methylenic chain of the inhibitor. Finally, besides water-mediated contacts with the carbonyl groups of Arg100 and Gly101, the positive charge of the piperidine unit in **5** appears to be stabilized by the carboxylate group of Glu84.

As noted above, treatment of MAO-A with **5** leads to a significant inactivation of the enzyme, which remains unaltered after repeated washings. In contrast, a significant recovery of MAO-B activity is found after washings because of a slower inactivation of this isoform. This different behavior suggests that the propargylamino moiety of **5** in MAO-A is better oriented for chemical modification of FAD than in MAO-B. Nevertheless, since both ligand and FAD are treated classically in MD simulations, the electronic effects that promote the chemical inactivation of the enzyme by the propargyl moiety are not properly accounted for. Therefore, we have compared the relative orientation of **5** obtained from MD simulations with the orientation found for clorgyline, deprenyl, rasagiline, and its ((ethyl(methyl)amino)carbonyl)oxy derivative (PDB entries 2BXR, 2BYB, 1S2Q, and 2C65),[67−69] paying attention to the relative positioning of the carbon atom attached to the protonated amine of **5** relative to the nitrogen atom of FAD involved in chemical modification by the irreversible inhibitors. Inspection of Figure 9 shows that in MAO-A such carbon atom is slightly closer to the FAD nitrogen atom than in MAO-B. Thus, the distance between those atoms (averaged over the snapshots sampled in the last 5 ns) amounts to 6.8 ± 0.3 Å in MAO-A and to 7.7 ± 0.4 Å in MAO-B (see Figure S13). The larger separation found in MAO-B agrees with the lower degree of enzyme inactivation found upon incubation with **5**.

To further check this assumption, we have run additional simulations forcing the nitrogen atom of the propargylamino group to occupy the position and orientation relative to FAD found for the corresponding atom in complexes of MAO-A with clorgyline, and MAO-B with deprenyl, rasagiline, and its ((ethyl(methyl)amino)carbonyl)oxy derivative (structurally related to ladostigil). Noteworthy, superposition of the X-ray structures of those complexes reveals that the nitrogen atom of the inhibitor occupies the same spatial location in the binding site, as expected from the similar geometrical arrangement of the propargylamino unit after chemical reaction with FAD (see Figure 9). To this end, restrained simulations (1 ns) were run in triplicate for each enzyme in order to force compound **5** to occupy the position expected after chemical reaction with FAD. With the aim to avoid artifactual results arising from steric clashes of the propargylamino group with binding site residues while steering the nitrogen atom, a methyl unit was used to replace the propargyl moiety. Finally, we have determined the difference in the interaction energy (from MM/PBSA calculations) between the inhibitor and the enzyme.

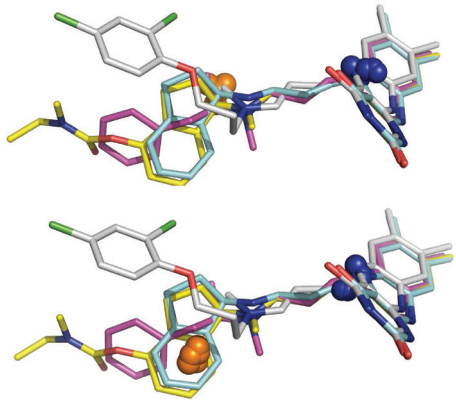

Figure 9. Superposition of the X-ray crystallographic structures of MAO-A complexed with clorgyline (white, PDB entry 2BXR) and MAO-B complexed with deprenyl (magenta, PDB entry 2BYB), rasagiline (blue, PDB entry 1S2Q), and its ((ethyl(methyl)amino)-carbonyl)oxy derivative (yellow, PDB entry 2C65). The spheres show the position of the carbon atom that bears the protonated amine of **5** (orange) and the chemically modified nitrogen atom of FAD (blue). Representation includes the positions of those atoms in snapshots taken every ns along the last 5 ns of the trajectory run for the complex (top) MAO-A−**5** and (bottom) MAO-B−**5**.

Figure 10 shows the time evolution of the distance between the ligand carbon atom (linked to the amino nitrogen) and the

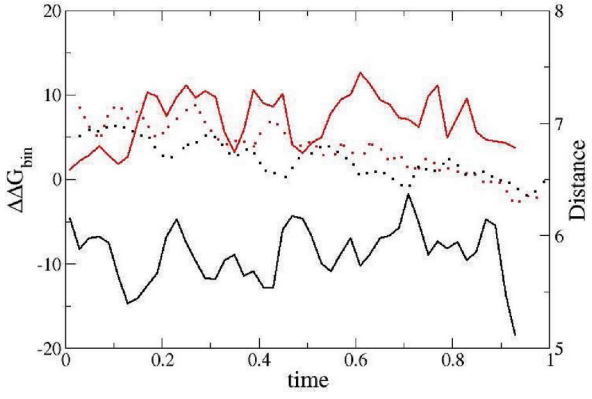

Figure 10. Time evolution of the distance between the ligand carbon atom (linked to the amino nitrogen) and the nitrogen atom of FAD along the restrained MD simulation (shown in dashed lines; MAO-A in black and MAO-B in red). The change in the interaction energy (estimated from MM/PBSA calculations) is shown by solid lines (MAO-A in black and MAO-B in red). For clarity of comparison, the interaction energy profiles are shown relative to the initial snapshot.

nitrogen atom of FAD along the restrained trajectories, and the corresponding change in the ligand−receptor interaction free energy estimated from MM/PBSA computations. The restrained simulations bring the nitrogen atom of **5** to the position expected for the covalent adduct with FAD (distance N(inhibitor)···N(FAD) at around 5.0 Å), the attached carbon atom being located at around 6.4 Å. Interestingly, the results indicate that the interaction energy in MAO-A becomes more negative (relative to the initial state) at around 7 kcal/mol, whereas it is destabilized at around 6 kcal/mol in MAO-B. Therefore, from a qualitative point of view, these results reinforce the notion that adoption of a reactive configuration of **5** in MAO-B is more impeded than in MAO-A, which agrees with the different rates of enzyme inactivation.

Finally, additional 20 ns MD simulations were run to simulate the adduct of **5** covalently bound to FAD. In the two cases MD simulations yielded stable trajectories, as noted by inspection of the time evolution of the potential energy (see Figure S14) and by the small fluctuations of the rmsd profile along the last 5 ns of the trajectories (see Figure 11). However,

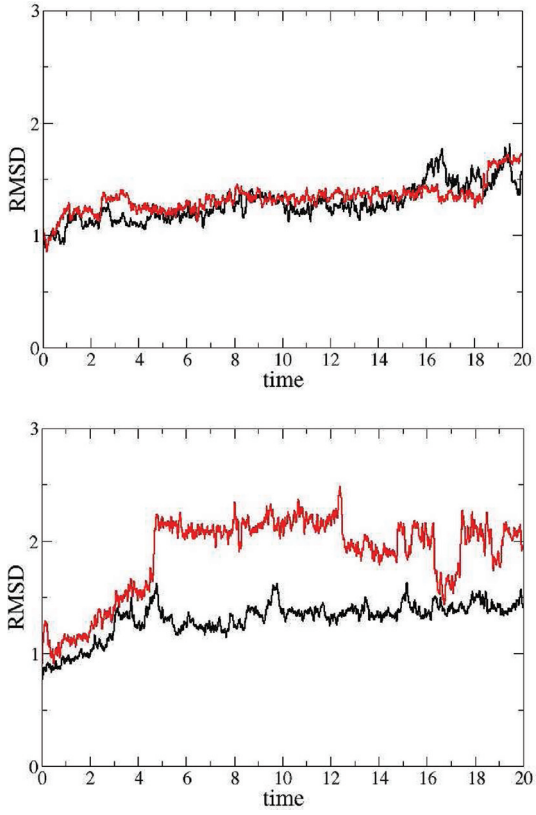

Figure 11. Time evolution of the rmsd determined for the backbone atoms (black) and the heavy atoms of the residues that define the binding site (red) along the trajectories run for the (top) MAO-A−**5** adduct and (bottom) MAO-A−**5** adduct.

it is also worth stressing the different profile of the rmsd along the whole trajectory. Thus, whereas there is a slight increase in the rmsd determined for both the backbone atoms and the heavy atoms of the residues that define the binding site in the simulation run for the MAO-A−**5** adduct (the rmsd increases from 1 to 1.5 Å; see Figure 11), there is a more abrupt increase in the rmsd determined for the binding site residues in the simulation run for the MAO-B−**5** adduct (the rmsd increases from 1 to 2.2 Å; see Figure 11). This trend agrees with the results derived from the restrained MD simulations discussed above and indicates that the proper accommodation of the inhibitor in a conformation suitable for covalent attachment to FAD requires a larger rearrangement in the binding site of MAO-B.

The different trends regarding the inhibitory activity of **5** in MAO-A and MAO-B can be mainly ascribed to the residues that define the bottleneck in the gorge that leads to the substrate binding site. In particular, the replacement of Ile199 in MAO-B by Phe208 in MAO-A pushes the inhibitor toward the FAD, whereas the replacement of Ile325 in MAO-A by Tyr326 in MAO-B triggers the opposite effect. Thus, even though there is a slight net stabilization in the interaction energy of the inhibitor covalently bound to FAD in both MAO-

dx.doi.org/10.1021/jm200853t | J. Med. Chem. 2011, 54, 8251−8270

A and MAO-B (relative to the noncovalent form; see Table S3), present results suggest that there is a larger barrier for the proper accommodation of **5** in MAO-B. In this context, though the methylenic (n = 2) tether designed for **5** seems well suited to fit the gorge in the two isoforms, the spatial constraints imposed on the orientation of the indole ring upon binding to MAO-B leads to a less effective chemical interaction with the FAD. In turn, these findings suggest that extension of the ((methyl)amino)propargylamino unit in **5** could be a useful strategy to enhance the inactivation of MAO-B while reducing the inhibition at MAO-A. This strategy could be beneficial to minimize side effects related to the potentiation of the cardiovascular effect of tyramine (the so-called "cheese effect"), a limited side effect of older generation of nonselective MAO inhibitors.

Inhibition of Aβ Self-Aggregation and AChE-Induced Aggregation. A number of dual binding site AChE inhibitors have been found to exhibit a significant inhibitory activity on Aβ self-aggregation.[60,70−75] Thus, compound **5** was also tested for its ability to inhibit the self-induced $A\beta_{1-42}$ aggregation and the AChE-induced $A\beta_{1-42}$ aggregation. In the former case a 47.8 ± 2.1% inhibition was found when compound **5** was tested at 10 μM (Table 3) (concentration ratio Aβ/inhibitor = 4/1).

Table 3. Inhibition of AChE-Induced $A\beta_{1-40}$ Aggregation and $A\beta_{1-42}$ Self-Induced Aggregation by Compound 5

	% inhibition of Aβ aggregation ± SEM	
compd	AChE-induced[a,c]	self-induced[b,c]
5	32.4 ± 7.0	47.8 ± 2.1

[a]Inhibition of AChE-induced $A\beta_{1-40}$ aggregation. The concentration of **5** and $A\beta_{1-40}$ was 100 and 40 μM, respectively. The ratio Aβ/AChE was equal to 100/1. [b]Inhibition of self-induced $A\beta_{1-42}$ aggregation (40 μM) produced by **5** at 10 μM. [c]Data are the mean ± SEM of at least three independent experiments.

We used propidium iodide (PI) as reference compound, and we obtained a reduction of Aβ self-induced aggregation of 33.3 ± 2.1%, this value being significantly lower than that found for **5**. When PI was tested at equimolar concentrations (Aβ/PI = 1/1), similar to that previously reported by other groups, we found a reduction of Aβ aggregation of 78.6 ± 3.8%. This effect is significantly higher than that reported for donepezil (<5%) under similar experimental conditions[72] and similar to that found for other IAChE.[60,71,72] Then **5** can be considered a moderate inhibitor of $A\beta_{1-42}$ self-induced aggregation. Regarding the inhibition of the human AChE-dependent $A\beta_{1-40}$ aggregation, the results indicate that **5** at 100 μM was able to prevent hAChE-induced $A\beta_{1-40}$ aggregation in a 32.4 ± 7.0% (Table 3). This value is similar to the inhibition elicited by donepezil (22%) and significantly higher than that found for tacrine (7%), two of the first FDA-approved drugs for the treatment of AD. However, it is significantly lower than that of propidium[76] and other IAChEs previously described,[70−72] which show potencies in the low micromolar range.

CONCLUSIONS

A new series of hybrid compounds containing the benzylpiperidine moiety of donepezil and the indolylpropargylamino moiety of *N*-[(5-benzyloxy-1-methyl-1*H*-indol-2-yl)methyl]-*N*-methylprop-2-yn-1-amine have been investigated as novel multitarget agents against AChE, BuChE, and MAO (A/B). These new compounds have been designed to simultaneously interact with the active, peripheral, and mid-gorge binding sites of AChE, as well as to occupy the substrate binding site in MAO.

The length of the tether that connects the two main structural fragments of the novel hybrids has a relevant effect on the binding to MAO, whereas it seems to have little impact on the inhibitory activity against AChE and BuChE. Among these hybrid compounds, **5** is the most potent IMAO, even more than the parent compounds. Surprisingly, although donepezil (**1**) is a slight inhibitor of BuChE and **2** is not even active, the ability of **5** to inhibit BuChE is found on the submicromolar range. This is particularly important in view of the renewed interest in dual cholinergic inhibitors as therapeutic agents for AD.[58] Normally, AChE predominates in the brain, while BuChE activity levels are low. However, in AD the relative enzymatic activity is altered such that BuChE increases while AChE decreases.[77,78] Then, if the therapeutic goal is to increase ACh levels in the brain, a compound able to inhibit both AChE and BuChE would be valuable to elicit a larger protective response. In addition, the inhibition of MAO-B by **5** might be beneficial for modulating the cholinergic neurotransmission and for restoring the serotoninergic neurotransmission. Moreover, the potent MAO-A inhibition enables the drug to exert an antidepressant activity like that of amitriptyline and moclobemide, two triciclic antidepressants primarily used to treat depression. Compound **5** also presents a significant inhibitory profile of Aβ-self-induced and human AChE-dependent aggregation, being more potent (human AChE-dependent) than or similar (self-induced) to the parent compound donepezil (**1**). Overall, the present data indicate that **5** not only is an interesting lead compound for the design of novel MTDL with a good IMAO/IAChE inhibitory potency and a significant activity against amyloid aggregation but also may have a potential disease-modifying role in the treatment of AD.

EXPERIMENTAL PART

General Methods. Melting points were determined in a Koffler apparatus and are uncorrected. ^{1}H NMR and ^{13}C NMR spectra were recorded at room temperature in $CDCl_3$ or DMSO-d_6 at 300, 400, or 500 MHz and at 75.4, 100.6, or 125.6 MHz, respectively, using solvent peaks [$CDCl_3$, 7.27 (D), 77.2 (C) ppm; DMSO-d_6, 2.50 (D) and 39.7 (C) ppm] as internal references. The assignment of chemical shifts is based on standard NMR experiments (^{1}H, ^{13}C, ^{1}H−^{1}H COSY, ^{1}H−^{13}C HSQC, HMBC, DEPT). Mass spectra were recorded on a GC/MS spectrometer with an API-ES ionization source. TLC was performed on silica F254. Detection was by UV light at 254 nm or by spraying with phosphomolybdic-H_2SO_4 dye reagent. Column chromatographies were performed on silica gel 60 (230 mesh). "Chromatotron" separations were performed on a Harrison Research model 7924. The circular disks were coated with Kieselgel 60 PF254 (E. Merck). The chlorydrate salts were prepared by solubilizing the compound in a minimum of ether, and a solution of ether saturated with HCl(g) was added dropwise. A white solid was formed immediately. The precipitated hydrochloride was separated by filtration, washed with ether, and dried. The purity (≥95%) of the samples was determined by elemental analysis, carried out at the IQOG (CSIC, Spain).

Methyl 4-(Piperidin-4-yl)butanoate (17).[55] A solution of (*E*)-ethyl 3-(pyridin-4-yl)acrylate **16**[52] (1.52 g, 8.58 mmol) in EtOH (20 mL) and 4 N HCl in 1,4-dioxane (2 mL) was hydrogenated under 10% Pd/C (0.152 g) and PtO_2 (152 mg) overnight at room temperature. Then the catalyst was filtered off, washed with MeOH, and the filtrate was concentrated. The residual solid was triturated with Et_2O, filtered, washed with Et_2O, and dried to give the known methyl

dx.doi.org/10.1021/jm200853t | J. Med. Chem. 2011, 54, 8251−8270

ester **17** (1.60 g, 90%) as a solid. ^{1}H NMR (300 MHz, DMSO-d_6) δ 9.29−9.10 (br, 2H), 3.55 (s, 3H, CO_2CH_3), 3.16−3.12 (m, 2H), 2.78−2.67 (m, 2H), 2.31−2.27 (m, 2H), 1.73−1.69 (m, 2H), 1.46−1.21 (m, 5H); MS (ES) m/z 172 $[M + H]^+$.

1-Benzyl-4-piperidinepropanol (19).[56] To a solution of methyl 4-(piperidin-4-yl)butanoate **17**[55] (1.60 g, 7.21 mmol) and benzyl bromide (1.85 g, 10.82 mmol) in 20 mL of CH_2Cl_2 was added triethylamine (3.3 mL, 21.65 mmol) while the internal temperature in the mixture was below 20 °C by cooling with an ice−water bath. The mixture was stirred at room temperature overnight. After complete reaction (TLC analysis), the mixture was concentrated and purified by column chromatography to give methyl 3-(1-benzylpiperidin-4-yl)propanoate (**18**) [(1.41 g, 75%): oil; ^{1}H NMR (300 MHz, $CDCl_3$) δ 7.35−7.23 (m, 5H), 3.66 (s, 3H, CO_2CH_3), 3.51 (s, 2H, CH_2-Ph), 2.89 (br d, J = 11.5 Hz, 2H), 2.32 (br t, J = 7.5 Hz, 2H, CH_2-CO_2CH_3), 1.94 (t, J = 10.9 Hz, 2H), 1.66−1.54 (m, 4H), 1.34−1.21 (m, 3H, CH + CH_2); MS (EI) m/z (%) 91 (100) $[PhCH_2]^+$, 188 (66) $[M - CH_2CH_2CO_2Me]^+$, 202 (13) $[M - CO_2Mt]^+$, 230 (19) $[M - OMe]^+$, 246 (9) $[M - CH_3]^+$, 260 (73) $[M - H]^+$, 261 (50) $[M]^+$], which was used in the next reaction without further analysis.

To a suspension of LAH (0.176 g, 4.66 mmol, 2 equiv) in dry THF (10 mL) was added methyl 3-(1-benzylpiperidin-4-yl)propanoate (**18**) (0.61 g, 2.33 mmol, 1 equiv) in dry THF (10 mL), at 0 °C. The mixture was refluxed for 2 h, and after cooling unreacted $LiAlH_4$ was quenched by careful addition of 10% NaOH solution (20 mL). The solution was filtered and washed with H_2O and EtOAc. The filtrate was extracted with EtOAc, and the combined organic layers, dried over Na_2SO_4, were concentrated to give known compound **19**[56] (0.535 g, 98%): oil; ^{1}H NMR (300 MHz, $CDCl_3$) δ 7.32−7.20 (m, 5H), 3.60 (t, J = 6.4 Hz, 2H, CH_2O), 3.48 (s, 2H, CH_2Ph), 2.87 (br d, J = 11.5 Hz, 2H), 1.92 (br d, J = 11.1 Hz, 2H), 1.68−1.60 (m, 2H), 1.61−1.49 (m, 2H), 1.30−1.15 (m, 5H); MS (EI) m/z (%): 91 (100) $[PhCH_2]^+$, 142 (26) $[M - CH_2Ph]^+$, 156 (17) $[M - Ph]^+$, 174 (8) $[M - (CH_2)_3OH]^+$, 188 (18) $[M - (CH_2)_2OH]^+$, 202 (14) $[M - CH_2OH]^+$, 232 (37) $[M - H]^+$, 233 (20) $[M]^+$.

1-Benzyl-4-(3-chloropropyl)piperidine (12). To a solution of 1-benzyl-4-piperidinepropanol (**19**)[56] (0.53 g, 2.27 mmol) in CH_2Cl_2 (5 mL), $SOCl_2$ (0.66 mL, 9.08 mmol, 4 equiv) was added dropwise with ice cooling. The mixture was refluxed for 3 h and then evaporated. The residue was rendered alkaline with 10% K_2CO_3 solution and extracted with CH_2Cl_2. The organic layer, dried over Na_2SO_4, was evaporated under reduced pressure to give compound **12** (0.582 g, 99%): oil; IR 3027, 2923, 2849, 2800, 2756, 1672, 1493, 1452, 1366, 1342, 1263, 738, 698 cm^{-1}; ^{1}H NMR (400 MHz, $CDCl_3$) δ 7.22−7.36 (m, 5H), 3.51 (t, J = 8.0 Hz, 2H, CH_2Cl), 3.51 (s, 2H, CH_2Ph), 2.89 (br d, J = 11.5 Hz, 2H), 1.95 (br t, J = 11.0 Hz, 2H), 1.78 (dt, J = 11.9 and 6.9 Hz, 2H, CH_2-CH_2Cl), 1.65 (br d, J = 11.4 Hz, 2H), 1.32−1.42 (m, 2H), 1.21−1.30 [m, 3H, CH + CH_2-$(CH_2)_2Cl$]; ^{13}C NMR (100 MHz, $CDCl_3$) δ 138.1 (C-Ph), 129.1 (2 × CH-Ph), 128.0 (CH-Ph), 126.8 (CH-Ph), 63.3 (CH_2-Ph), 53.6 ($2CH_2$-piperidine), 45.2 (CH_2Cl), 35.1 (CH), 33.6 [CH_2-$(CH_2)_2Cl$], 32.1 ($2CH_2$-pieridine), 29.9 (CH_2, CH_2-CH_2Cl); MS (EI) m/z (%) 91 (100) $[PhCH_2]^+$, 160 (23) $[M - Bn]^+$, 174 (27) $[M - (CH_2)_3Cl]^+$, 188 (17) $[M - (CH_2)_2Cl]^+$, 202 (9) $[M - CH_2Cl]^+$, 216 (88) $[M - Cl]^+$, 250 (35) $[M - 1]^+$. Anal. Calcd for $C_{15}H_{22}ClN$: C, 71.55; H, 8.81; N, 5.56. Found: C, 71.84; H, 9.02; N, 5.83.

1-Benzyl-4-(4-chlorobutyl)piperidine (13). To a solution of 1-benzyl-4-(4-hydroxybutyl)piperidine (**24**)[57] (0.508 g, 2.05 mmol) in CH_2Cl_2 (5 mL), $SOCl_2$ (0.6 mL, 8.214 mmol, 4 equiv) was added dropwise with ice cooling. The mixture was refluxed for 2 h and then evaporated. The residue was rendered alkaline with 10% K_2CO_3 solution and extracted with CH_2Cl_2. The organic layer, dried over Na_2SO_4, was evaporated under reduced pressure to give compound **13** (0.54 g, 99%) as a yellow oil. IR 3062, 3027, 2921, 2847, 2799, 2757, 1493, 1454, 1366, 1341, 1311, 1287, 1126, 1073, 1029, 979, 737, 698 cm^{-1}; ^{1}H NMR (300 MHz, $CDCl_3$) δ 7.34−7.21 (m, 5H), 3.53 (t, J = 6.7 Hz, 2H, CH_2Cl), 3.50 (s, 2H, CH_2Ph), 2.88 (br d, J = 11.4 Hz, 2H), 1.93 (br t, J = 11.9 Hz, 2H), 1.75 (tt, J = 8 Hz, 2H, CH_2-CH_2Cl), 1.70−1.59 (m, 2H), 1.49−1.37 (m, 2H), 130−1.20 (m, 5H); ^{13}C NMR (100 MHz, $CDCl_3$) δ 32.2 ($2CH_2$), 32.7 (CH_2, CH_2-CH_2Cl), 32.8 (CH_2), 36.2 (CH_2), 45.0 (CH_2Cl), 53.8 ($2CH_2$), 63.4 (CH_2-Ph), 126.8 (CH-Ph), 128.0 (2 × CH-Ph), 129.1 (2 × CH-Ph), 138.3 (C-Ph); MS (EI) m/z (%) 91 (100) $[PhCH_2]^+$, 174 (42) $[M - (CH_2)_4Cl]^+$, 188 (43) $[M - (CH_2)_3Cl]^+$, 202 (16) $[M - (CH_2)_2Cl]^+$, 216 (8) $[M - CH_2Cl]^+$, 230 (28) $[M - Cl]^+$, 264 (45) $[M]^+$. HRMS (ES+), exact mass calcd for $C_{16}H_{25}ClN$ $(M + H)^+$: 266,1676. Found: m/z 266.1687.

***N*-((5-((1-Benzylpiperidin-4-yl)methoxy)-1-methyl-1*H*-indol-2-yl)methyl)-*N*-methylprop-2-yn-1-amine (3).** To a solution of 1-methyl-2-{[ethyl(prop-2-yn-1-yl)amino]ethyl}-1*H*-indol-5-ol **4**[52] (0.21 g, 0.94 mmol) and 1-benzyl-4-(chloromethyl)piperidine **10**[27] (0.33 g, 1.51 mmol, 1.5 equiv) in acetonitrile (5 mL), NaH (120 mg, 3 mmol, 3 equiv, 60% mineral oil) was added. The reaction mixture was stirred at 50 °C for 10 h. After complete reaction (TLC analysis), the mixture was concentrated, diluted with water, and extracted with CH_2Cl_2. The organic phase was washed with brine, dried ($MgSO_4$), and evaporated. The crude product was purified by flash chromatography (CH_2Cl_2/MeOH, 100:1) to give compound **3** (126.3 mg, 32%) as white solid: R_f = 0.24 (CH_2Cl_2/MeOH, 10:1); mp 123−5 °C; IR (KBr) ν 3252, 2938, 2913, 1620, 1489, 1466, 1195, 1163, 1029, 1008 cm^{-1}; ^{1}H NMR (400 MHz, $CDCl_3$) δ 7.35−7.24 (m, 5H), 7.18 (d, J = 8.8 Hz, 1H, CH7-indole), 7.04 (d, J = 2.3 Hz, 1H, CH4-indole), 6.86 (dd, J = 8.8 and 2.3 Hz, 1H, CH6-indole), 6.34 (s, 1H, CH3-indole), 3.85 (d, J = 6.0 Hz, 2H, -CH_2O-), 3.73 (s, 3H, N-CH_3), 3.68 (s, 2H, indole-CH_2-N), 3.53 (s, 2H, CH_2-Ph), 3.31 (d, 2H, J = 2.2 Hz, CH_2-C≡CH), 2.95 (d, J = 11.4 Hz, 2H), 2.35 (s, 3H, N-CH_3), 2.30 (t, J = 2.2 Hz, C≡CH), 2.02 (t, J = 16, 2H), 1.91−1.81 (m, 3H), 1.49−1.39 (m, 2H); ^{13}C NMR (100 MHz, $CDCl_3$) δ 153.3 (C5-indole), 138.3 (C1′-Ph), 137.8 (C2-indole), 133.3 (C7a-indole), 129.1 (2 × CH-Ph), 128.1 (2 × CH-Ph), 127.5 (C3a-indole), 126.8 (CH4′-Ph), 111.9 (CH6-indole), 109.5 (CH7-indole), 103.3 (CH4-indole), 102.0 (CH3-indole), 78.4 (-C≡), 73.6 (CH_2-O), 73.4 (≡CH), 63.4 (CH_2-Ph), 54.0 (2 × CH_2), 63.4 (Ph-CH_2), 53.4 (2 × CH_2), 51.7 (Ind-CH_2-N), 44.6 (CH_2-C≡), 41.5 (N-CH_3), 35.9 (CH-piperidine), 29.8 (N-CH_3), 29.1 (2 × CH_2); MS (EI) m/z (%) 416 (100) $[M + H]^+$, 438 (2) $[M + Na]^+$. **3**·2HCl: white powder; mp 230−3 °C; IR (KBr) ν 3423, 3200, 2933, 2511, 1620, 1486, 1466, 1208 cm^{-1}; ^{1}H NMR (300 MHz, D_2O) δ 7.34−7.25 (m, 6H, CH7-indole + 5H-Ph), 7.05 (d, J = 2.2 Hz, 1H, CH4-indole), 6.85 (dd, J = 9.0, 2.2 Hz, 1H, CH6-indole), 6.59 (s, 1H, CH3-indole), 4.47 (s, 2H, CH_2), 4.11 (s, 2H, CH_2), 3.86 (d, J = 2.4 Hz, 2H, CH_2-C≡CH), 3.79 (t, J = 6.0 Hz, 2H, O-CH_2-), 3.59 (s, 3H, indole-CH_3), 3.38 (d, J = 12.8 Hz, 2H, CH_2), 2.97 (t, J = 2.3 Hz, 1H, C≡CH), 2.85 (t, J = 12.7 Hz, 2H, CH_2), 2.76 (s, 3H, N-CH_3), 1.98 (d, J = 12.8 Hz, 2H, CH_2), 1.89−1.83 (m, 1H, CH), 1.48−1.34 (m, 2H, CH_2). Anal. Calcd for $C_{27}H_{35}Cl_2N_3O$: C, 66.39; H, 7.22; Cl, 14.52; N, 8.60. Found: C, 66.21; H, 7.43; Cl, 14.42; N, 8.63.

***N*-{[5-(2-(1-Benzylpiperidin-4-yl)ethoxy)-1-methyl-1*H*-indol-2-yl]methyl}-*N*-methylprop-2-yn-1-amine (4).** To a solution of 1-methyl-2-{[ethyl(prop-2-yn-1-yl)amino]ethyl}-1*H*-indol-5-ol **14**[52] (160 mg, 0.7 mmol) and 1-benzyl-4-(2-chloroethyl)piperidine **11**[53] (0.25 g, 1.05 mmol, 1.5 equiv) in DMF (5 mL), NaH (84 mg, 2.1 mmol, 3 equiv, 60% mineral oil) was added. The reaction mixture was stirred at room temperature for 3 h. After complete reaction, the solvent was removed and the crude was diluted with water and extracted with CH_2Cl_2. The organic phase was washed with brine, dried ($MgSO_4$), and evaporated at reduced pressure. The crude product was purified by flash chromatography (CH_2Cl_2/MeOH, 100:1) to give compound **4** (0.216 g, 72%) as a white solid: R_f = 0.27 (CH_2Cl_2/MeOH, 10:1); mp 86−7 °C; IR (KBr) ν 3275, 2941, 2921, 2876, 2807, 2782, 2768, 1619, 1488, 1473, 1289, 1250, 1207, 1161, 1030 cm^{-1}; ^{1}H NMR (400 MHz, $CDCl_3$) δ 7.34−7.23 (m, 5H), 7.18 (d, J = 8.8 Hz, 1H, CH7-indole), 7.03 (d, J = 2.4 Hz, 1H, CH4-indole), 6.85 (dd, J = 8.8 and 2.4 Hz, 1H, CH6-indole), 6.33 (s, 1H, CH3-indole), 4.03 (t, J = 6.5 Hz, 2H, O-CH_2-), 3.74 (s, 3H, N-CH_3), 3.67 (s, 2H, N-CH_2), 3.52 (s, 2H, CH_2-Ph), 3.31 (d, 2H, J = 2.3 Hz, CH_2-C≡CH), 2.91 (d, J = 11.6 Hz, 2H), 2.34 (s, 3H, N-CH_3), 2.29 (t, J = 2.3 Hz, C≡CH), 2.0 (t, J = 10.8, 2H), 1.77−1.72 (m, 4H), 1.41−1.31 (m, 2H), 1.62−1.52 (m, CH); ^{13}C NMR (100 MHz, $CDCl_3$) δ 153.5 (C5-indole), 138.4 (C-Ph), 133.6 (C-indole), 137.2 (C-indole), 129.5

(2 × CH-Ph), 128.3 (2 × CH-Ph), 127.7 (C-indole), 127.2 (CH-Ph), 112.2 (CH6-indole), 109.5 (CH7-indole), 103.5 (CH4-indole), 102.0 (CH3-indole), 78.6 (-C≡), 73.6 (≡CH), 66.7 (CH_2-O), 63.6 (CH_2-Ph), 53.9 (2 × CH_2), 52.0 (CH_2-indole), 44.9 (CH_2-C≡CH), 41.8 (N-CH_3), 36.2 (CH_2), 32.8 (CH_2), 32.4 (CH_2), 30.1 (N-CH_3); MS (EI) *m/z* (%) 91 (48) $[PhCH_2]^+$, 202 (100), 361 (3) $[M - NCH_3CH_2C{\equiv}CH)]^+$, 429 (4) $[M]^+$. Anal. Calcd for $C_{28}H_{35}N_3O$: C, 78.28; H, 8.21; N, 9.78. Found: C, 77.99; H, 8.45; N, 9.79. **4**·2HCl: white powder; mp 221−3 °C; IR (KBr) ν 3424, 3195, 2928, 2561, 2506, 1619, 1486, 1471, 1210 cm^{-1}; ^1H NMR (300 MHz, D_2O) δ 7.33−7.25 (m, 6H, CH7-indole + 5H-Ph), 7.06 (d, *J* = 2.4 Hz, 1H, CH4-indole), 6.84 (dd, *J* = 9.0, 2.4 Hz, 1H, CH6-indole), 6.58 (s, 1H, CH3-indole), 4.45 (s, 2H, CH_2), 4.08 (s, 2H, CH_2), 3.96 (t, *J* = 6.2 Hz, 2H, O-CH_2-), 3.84 (d, *J* = 2.4 Hz, 2H, CH_2-C≡CH), 3.59 (s, 3H, indole-CH_3), 3.32 (d, *J* = 12.6 Hz, 2H, CH_2), 2.96 (t, *J* = 2.4 Hz, 1H, C≡CH), 2.85−2.75 (m 5H, CH_2 + N-CH_3), 1.84 (d, *J* = 13.6 Hz, 2H, CH_2), 1.75−1.63 [m, 1H, CH], 1.61−1.53 (m, 2H, CH_2-CH_2O-), 1.32−1.18 (m, 2H, CH_2). Anal. Calcd for $C_{28}H_{35}N_3O{\cdot}2HCl{\cdot}^1/_3(H_2O)$: C, 66.13; H, 7.47; Cl, 13.94; N, 8.26. Found: C, 66.04; H, 7.89; Cl, 13.84; N, 8.59.

***N*-{[5-(3-(1-Benzylpiperidin-4-yl)propoxy)-1-methyl-1*H*-indol-2-yl]methyl}-*N*-methylprop-2-yn-1-amine (5).** To a solution of 1-methyl-2-{[ethyl(prop-2-yn-1-yl)amino]ethyl}-1*H*-indol-5-ol **4**[52] (0.22 g, 0.963 mmol) and 1-nenzyl-4-(3-chloropropyl)piperidine **12** (0.36 g, 1.44 mmol, 1.5 equiv) in DMF (5 mL), NaH (69.4 mg, 1.73 mmol, 1.8 equiv, 60% /mineral) was added. The reaction mixture was stirred at room temperature overnight and then heated at 100 °C for 1 h. After complete reaction (TLC analysis), the mixture was concentrated, diluted with water, and extracted with CH_2Cl_2. The organic phase was washed with brine, dried ($MgSO_4$), and evaporated at reduced pressure. The crude product was purified by flash chromatography (CH_2Cl_2/AcOEt, 10:1 to 5:1, v/v) to give compound **5** (0.268 g, 63%) as a white solid: R_f = 0.28 (CH_2Cl_2/MeOH, 20:1); mp 90−91 °C; IR (KBr) ν 3265, 2935, 2908, 2799, 2760, 1619, 1489, 1471, 1395, 1269, 1204, 1190, 1160, 1029 cm^{-1}; ^1H NMR (400 MHz, $CDCl_3$) δ 7.35−7.25 (m, 5H, Ph), 7.19 (d, *J* = 8.8 Hz, 1H, CH7-indole), 7.05 (d, *J* = 2.14 Hz, 1H, CH4-indole), 6.85 (dd, *J* = 8.8 and 2.3 Hz, 1H, CH6-indole), 6.35 (s, 1H, CH3-indole), 3.98 (t, *J* = 6.6 Hz, 2H, O-CH_2-), 3.75 (s, 3H, indole-CH_3), 3.69 (s, 2H, indole-CH_2), 3.52 (s, 2H, CH_2-Ph), 2.33 (d, *J* = 2.2 Hz, 2H, CH_2-C≡CH), 2.91 (d, *J* = 10.8 Hz, CH_2), 2.36 (s, 3H, N-CH_3), 2.31 (t, *J* = 2.0 Hz, C≡CH), 1.97 (t, *J* = 12 Hz, 2H, CH_2), 1.83 [m, 2H, CH_2-(CH_2O)], 1.72 (d, *J* = 9.1 Hz, 2H, CH_2), 1.46−1.41 [m, 2H, CH_2-(CH_2)$_2$O], 1.29−1.31 (m, 3H, CH+CH_2); ^{13}C NMR (100 MHz, $CDCl_3$) δ 153.2 (C5-indole), 138.3 (C-Ph), 136.9 (C2-indole), 133.3 (C-indole), 129.2 (2 × CH-Ph), 128.0 (2 × CH-Ph), 127.4 (C-indole), 126.8 (CH-Ph), 112.0 (CH6-indole), 109.5 (CH7-indole), 103.3 (CH4-indole), 102.0 (CH3-indole), 78.3 (-C≡), 73.4 (≡CH), 69.0 (CH_2-O), 63.4 (CH_2-Ph), 53.8 (2 × CH_2), 51.7 (indole-CH_2), 44.6 (CH_2-C≡), 41.5 (N-CH_3), 35.5 (CH-piperidine), 32.8 [CH_2-(CH_2)$_2$O], 32.2 (2CH_2), 29.8 (indole-N-CH_3), 26.7 [CH_2-CH_2O]; MS (EI) *m/z* (%) 91 (77) $[PhCH_2]^+$, 352 (22) $[M - CH_2Ph]^+$, 374 (100) $[M - NCH_3CH_2C{\equiv}CH)]^+$, 404 (7) $[M - CH_2C{\equiv}CH)]^+$, 428 (5) $[M - CH_3]^+$, 443 (40)$[M]^+$. Anal. Calcd for $C_{29}H_{37}N_3O$: C, 78.51; H, 8.41; N, 9.47. Found: C, 78.36; H, 8.31; N, 9.23. **5**·2HCl: white powder; mp 203−5 °C; IR (KBr) ν 3193, 2937, 2512, 1619, 1486, 1469, 1209 cm^{-1}; ^1H NMR (300 MHz, D_2O) δ 7.32−7.22 (m, 6H, CH7-indole + 5H-Ph), 7.05 (d, *J* = 2.2 Hz, 1H, CH4-indole), 6.83 (dd, *J* = 9.0, 2.3 Hz, 1H, CH6-indole), 6.58 (s, 1H, CH3-indole), 4.45 (s, 2H, CH_2), 4.07 (s, 2H, CH_2), 3.90 (t, *J* = 6.1 Hz, 2H, O-CH_2-), 3.83 (d, *J* = 2.2 Hz, 2H, CH_2-C≡CH), 3.59 (s, 3H, indole-CH_3), 3.30 (d, *J* = 12.0 Hz, 2H, CH_2), 2.97−2.94 (m, 1H, C≡CH), 2.81−2.72 (m 5H, CH_2 + N-CH_3), 1.84−1.75 (m, 2H, CH_2), 1.65−1.55 (m, 2H, CH_2), 1.49−1.36 (m, 1H, CH), 1.41−1.46 [m, 2H, CH_2-(CH_2)$_2$O], 1.29−1.09 (m, 4H). Anal. Calcd for $C_{29}H_{37}N_3O{\cdot}2HCl$: C, 67.43; H, 7.61; Cl, 13.73; N, 8.13. Found: C, 67.38; H, 7.81; Cl, 13.13; N, 8.02.

***N*-{[5-(4-(1-Benzylpiperidin-4-yl)butoxy)-1-methyl-1*H*-indol-2-yl]methyl}-*N*-methylprop-2-yn-1-amine (6).** To a solution of 1-methyl-2-{[ethyl(prop-2-yn-1-yl)amino]ethyl}-1*H*-indol-5-ol **4**[52] (0.35 g, 1.56 mmol) and 1-benzyl-4-(4-chlorobutyl)piperidine **13** (0.5 g, 1.88 mmol, 1.2 equiv) in 8 mL of DMF, NaH (0.1 g, 2.5 mol, 1.6 equiv, 60% mineral oil) was added. The reaction mixture was stirred at room temperature overnight and then heated at 70 °C for 8 h. Then the mixture was concentrated, diluted with water, and extracted with CH_2Cl_2. The organic phase was washed with brine, dried ($MgSO_4$), and evaporated. The crude product was purified by flash chromatography (CH_2Cl_2/MeOH, 50:1 to 30:1, v/v) to give compound **6** (0.547 g, 76%) as a white solid: R_f = 0.28 (CH_2Cl_2/MeOH, 20:1); mp 93−94 °C; IR (KBr) ν 3260, 2937, 2918, 1619, 1489, 1472, 1203, 1193, 1160, 1008 cm^{-1}; ^1H NMR (500 MHz, $CDCl_3$) δ 7.32−7.23 (m, 5H), 7.17 (d, *J* = 8.8 Hz, 1H, CH7-indole), 7.03 (d, *J* = 2.3 Hz, 1H, CH4-indole), 6.85 (dd, *J* = 8.8 and 2.4 Hz, 1H, CH6-indole), 6.32 (s, 1H, CH3-indole), 3.98 (t, *J* = 6.6 Hz, 2H, -CH_2O-), 3.67 (s, 2H, CH_2-N), 3.73 (s, 3H, N-CH_3), 3.49 (s, 2H, CH_2-Ph), 3.31 (d, *J* = 2.4 Hz, CH_2-C≡CH, 2H), 2.88 (d, *J* = 10.5 Hz, 2H, CH_2pip), 2.34 (s, 3H, N-CH_3), 2.28 (t, *J* = 2.4 Hz, 1H, C≡CH), 2.00−1.85 (m, 2H, CH_2pip), 1.83−1.73 (m, 2H, CH_2-CH_2O), 1.66 (br d, *J* = 9.4 Hz, CH_2pip), 1.51−1.45 (m, 2H, CH_2-(CH_2)$_2$O), 1.34−1.22 (M, 4H, CH_2pip + CH_2-(CH_2)$_3$O); ^{13}C NMR (125 MHz, $CDCl_3$) δ 153.5 (C5-indole) 138.5 (C-Ph), 137.0 (C2-indole), 133.3 (C7a-indole), 129.2 (2 × CH_2Ph), 128.1 (2 × CHPh), 127.5 (C3a-indole), 126.8 (CH-Ph), 112.0 (CH6-indole), 109.5 (CH7-indole), 103.4 (CH4-indole), 102.0 (CH_3-indole), 78.4 (-C≡), 73.4 (≡CH), 68.8 (CH_2-O), 63.5 (CH_2-Ph), 53.9 (2 × CH_2-piperidine), 51.8 (N-CH_2-indole), 44.7 (CH_2-C≡CH), 41.7 (N-CH_3), 36.3 (CH_2-(CH_2)$_3$O), 35.6 (CH-piperidine), 32.3 (2 × CH_2-piperidine), 29.8 (N-CH_3), 29.7 (CH_2-CH_2O), 23.3 [CH_2-(CH_2)$_2$O]; MS (EI) *m/z* (%) 91 (55) $[PhCH_2]^+$, 172 (71), 228 (45), 366 (41) $[M - Bn]^+$, 388 $[M - NCH_3CH_2C{\equiv}CH)]^+$, 418 (8) $[M - CH_2C{\equiv}CH)]^+$, 457 (26) $[M]^+$. Anal. Calcd for $C_{30}H_{39}N_3O$: C, 78.73; H, 8.59; N, 9.18. Found: C, 78.65; H, 8.71; N, 9.07. **6**·2HCl: white powder; mp 197−9 °C; IR (KBr) ν 3421, 3195, 2928, 2851, 2561, 2509, 1619, 1485, 1472, 1458, 1408, 1209 cm^{-1}; ^1H NMR (300 MHz, D_2O) δ 7.33−7.24 (m, 6H, CH7-ind + 5H-Ph), 7.05 (d, *J* = 2.2 Hz, 1H, CH4-ind), 6.84 (dd, *J* = 9.0, 2.4 Hz, 1H, CH6-ind), 6.59 (s, 1H, CH3-ind), 4.48 (s, 2H, CH_2), 4.05 (s, 2H, CH_2), 3.90 (t, *J* = 6.5 Hz, 2H, O-CH_2-), 3.86 (d, *J* = 2.2 Hz, 2H, CH_2-C≡CH), 3.58 (s, 3H, indole-CH_3), 3.28 (d, *J* = 12.3 Hz, 2H, CH_2), 2.98 (t, *J* = 2.3 Hz, 1H, C≡CH), 2.77−2.70 (m 5H, CH_2 + N-CH_3), 1.76 (d, *J* = 13.9 Hz, 2H, CH_2), 1.61−1.51 (m, 2H, CH_2), 1.41−1.23 (m, 3H, CH + CH_2), 1.29−1.05 (m, 4H). Anal. Calcd for $C_{30}H_{39}N_3O{\cdot}2HCl$: C, 67.91; H, 7.79; Cl, 13.36; N, 7.92. Found: C, 67.54; H, 7.45; Cl, 13.25; N, 8.10;

***N*-{[5-(2-Bromoethoxy)-1-methyl-1*H*-indol-2-yl)methyl}-*N*-methylprop-2-yn-1-amine (25).** A mixture of 1-methyl-2-{[ethyl-(prop-2-yn-1-yl)amino]ethyl}-1*H*-indol-5-ol **14**[52] (0.215 g, 0.942 mmol), 1,2-dibromoethane (1.77 g, 9.42 mmol), and potassium carbonate (0.65 g, 4.71 mmol) in 2-butanone (8 mL) was reacted at 85 °C for 6 h. The mixture was evaporated in vacuo, and the residue was partitioned between dichloromethane (10 mL) and water (10 mL). The organic layer was dried (Na_2SO_4) and evaporated. The residue was purified by column chromatography, eluting with 4% methanol in dichloromethane, affording compound **25** (117.3 mg, 37%): R_f = 0.76 (CH_2Cl_2/AcOEt, 10:1); mp 75−77 °C; IR 3274, 29712937, 2877, 2800, 1619, 1579, 1488, 1473, 1400, 1267, 1205, 1198, 1159, 1118, 1025, 889, 842, 794, 776, 690 cm^{-1}; ^1H NMR (300 MHz, $CDCl_3$) δ 7.2 (d, *J* = 8.8 Hz, 1H, CH7-indole), 7.07 (d, *J* = 2.4 Hz, 1H, CH4-indole), 6.9 (dd, *J* = 8.8, 2.5 Hz, 1H, CH6-indole), 6.36 (s, 1H, CH3-indole), 4.33 (t, *J* = 6.4 Hz, 2H, -CH_2-O-), 3.75 (s, 3H, N-CH_3), 3.69 (s, 2H, N-CH_2), 3.66 (t, *J* = 6.4 Hz, 2H, -CH_2-Br), 3.32 (d, *J* = 2.4 Hz, 2H, N-CH_2-C≡), 2.36 (s, 3H, N-CH_3), 2.31 (t, *J* = 2.4 Hz, 1H, ≡CH); ^{13}C NMR (75 MHz, $CDCl_3$) δ 152.2 (C5-indole), 137.3 (C2-indole), 133.8 (C7a-indole), 127.4 (C3a-indole), 112.2 (CH6-indole), 109.7 (CH7-indole), 104.4 (CH4-indole), 102.1 (CH3-indole), 78.3 (-C≡), 73.5 (≡CH), 69.1 (CH_2-O), 51.7 (CH_2-N), 44.7 (-CH_2-C≡), 41.5 (N-CH_3), 29.9 (N-CH_3), 29.6 (CH_2-Br); MS (EI) *m/z*(%): 131 (48), 160 (66) $[M - ((Br(CH_2)_2)$-$NCH_3CH_2C{\equiv}CH)]^+$, 267 (100) $[M - NCH_3CH_2C{\equiv}CH)]^+$, 334 (25)$[M]^+$. Anal. Calcd for $C_{16}H_{19}BrN_2O$: C, 57.32; H, 5.71; Br, 23.83; N, 8.36. Found: C, 57.50; H, 5.70; Br, 23.24; N, 8.54.

dx.doi.org/10.1021/jm200853t | *J. Med. Chem.* 2011, 54, 8251−8270

***N*-{[5-(2-(4-Benzylpiperidin-1-yl)ethoxy)-1-methyl-1*H*-indol-2-yl]methyl}-*N*-methylprop-2-yn-1-amine (7).** 4-Benzylpiperidine (36 μL, 0.2 mmol) was added to a mixture of **25** (34 mg, 0.1 mmol) and potassium carbonate (42 mg, 0.3 mmol) in *N*,*N*-dimethylformamide (1 mL). The reactants were heated at 80 °C overnight under an atmosphere of argon. The reaction mixture was poured into water (5 mL) and extracted with dichloromethane (3 × 20 mL). The organic layers were combined, dried (Na_2SO_4), and concentrated. The residue was purified by column chromatography, eluting with 3.3% methanol in dichloromethane, affording compound **7** (33.5 mg, 77%): white solid; R_f = 0.49 (CH_2Cl_2/MeOH, 10:1); ^{1}H NMR (400 MHz, $CDCl_3$) δ 7.31−7.25 (m, 2H), 7.23−7.14 (m, 4H), 7.06 (d, *J* = 2.36 Hz, 1H, CH4-indole), 6.88 (dd, *J* = 8.83 and 2.43 Hz, 1H, CH6-indole), 6.35 (s, 1H, CH3-indole), 4.16 (t, *J* = 6.06 Hz, 2H, -CH_2-O), 3.74 (s, 3H, CH_3), 3.68 (s, 2H, N-CH_2), 3.32 (d, *J* = 2.35 Hz, 2H, CH_2), 3.034 (d, *J* = 11.7 Hz, CH_2), 2.83 (t, *J* = 6.03 Hz, CH_2), 2.56 (d, *J* = 7.016 Hz, CH_2), 2.35 (s, 3H, CH_3), 2.31 (t, *J* = 2.37 Hz, C≡CH), 2.086 (td, *J* = 11.77, 2.18 Hz, 1H, CH_2), 1.67 (d, *J* = 12.87 Hz, CH_2), 1.56 (m, CH), 1.38 (qd, *J* = 12.15, 3.79 Hz, CH_2); ^{13}C NMR (100 MHz, $CDCl_3$) δ 152.9 (C5-indole), 140.6 (C-Ph), 137.0 (C2-indole), 133.3 (C7a-indole), 129.0 (2 × CH-Ph), 128.0 (2 × CH-Ph), 127.4 (C3a-indole), 125.7 (CH-Ph), 111.0 (CH6-indole), 109.5 (CH7-indole), 103.4 (CH4-indole), 102.0 (CH3-indole), 78.3 (≡CH), 73.4 (-C≡), 66.6 (CH_2O), 57.6 (CH_2), 54.2 (2 × CH_2), 51.7 (indole-CH_2), 44.65 (CH_2), 43.1 (CH_2), 41.5 (N-CH_3), 37.67 (CH), 32.0 (2 × CH_2), 29.8 (CH_3); MS (EI) *m*/*z* (%) 188 (100), 202 (42), 429 (6)[M]$^+$. **7**·2HCl: white powder; mp 218−220 °C; IR (KBr) ν 3421, 3189, 2929, 2498, 1619, 1486, 1208, 1163 cm^{-1}; ^{1}H NMR (300 MHz, D_2O) δ 7.28 (d, *J* = 8.9 Hz, 1H, CH7-indole), 7.20−7.15 (m, 2H), 7.10−7.06 (m, 4H), 6.87 (dd, *J* = 9.0, 1.9 Hz, 1H, CH6-indole), 6.61 (s, 1H, CH3-indole), 4.49 (s, 2H, CH_2), 4.25−4.13 (m, 2H, -CH_2O), 3.87 (d, *J* = 1.8 Hz, 2H, CH_2), 3.60 (s, 3H, CH_3), 3.47 (d, *J* = 12.2 Hz, 2H, CH_2), 3.39−3.30 (m, 2H, CH_2), 2.98 (t, *J* = 1.9 Hz, 1H, C≡CH), 2.87−2.77 (m, 5H, CH_2 + N-CH_3), 2.43 (d, *J* = 6.6 Hz, 2H, CH_2), 1.75−1.71 (m, 3H, CH + CH_2), 1.41−1.28 (m, 2H, CH_2). Anal. Calcd for $C_{28}H_{37}Cl_2N_3O\cdot{}^2/_3(H_2O)$: C, 65.36; H, 7.51; N, 8.17. Found: C, 65.08; H, 7.74; N, 8.40.

***N*-{[5-(3-Bromopropoxy)-1-methyl-1*H*-indol-2-yl]methyl}-*N*-methylprop-2-yn-1-amine (26).** A mixture of 1-methyl-2-{[ethyl-(prop-2-yn-1-yl)amino]ethyl}-1*H*-indol-5-ol **14**[52] (21 mg, 0.092 mmol), 1,3-dibromopropane (186 mg, 0.92 mmol), and potassium carbonate (64 mg, 0.46 mmol) in 2-butanone (1 mL) was reacted at 85 °C for 6 h. The mixture was evaporated, and the residue was partitioned between dichloromethane (10 mL) and water (10 mL). The organic layer was dried (Na_2SO_4) and evaporated in vacuo to give compound **26** (25.4 mg, 80%): R_f = 0.62 (CH_2Cl_2/AcOEt, 10:1); mp 71−2 °C; IR (KBr) ν 3275, 1488, 1468, 1206, 1026 cm^{-1}; ^{1}H NMR (400 MHz, $CDCl_3$) δ 7.2 (d, *J* = 8.9 Hz, 1H, CH7-indole), 7.07 (d, *J* = 2.4 Hz, 1H, CH4-indole), 6.87 (dd, *J* = 8.8 and 2.4 Hz, 1H, CH6-indole), 6.35 (s, 1H, CH3-indole), 4.14 (t, *J* = 5.8 Hz, 2H, -CH_2-OH), 3.75 (s, 3H, N-CH_3), 3.69 (s, 2H, ind-CH_2-N), 3.65 (t, *J* = 6.5 Hz, 2H, -CH_2-Br), 3.32 (d, *J* = 2.4 Hz, 2H, CH_2-C≡), 2.36 (s, 3H, N-CH_3), 2.33 [t, *J* = 5.9 Hz, CH_2-(CH_2O)], 2.30 (t, *J* = 2.4 Hz, 1H, ≡CH); ^{13}C NMR (100 MHz, $CDCl_3$) δ 152.8 (C5-indole), 137.1 (C2-indole), 133.5 (C7a-indole), 127.2 (C3a-indole), 111.9 (CH6-indole), 109.6 (CH7-indole), 103.6 (CH4-indole), 102.1 (CH3-indole), 78.3 (-C≡), 73.4 (≡CH), 66.3 (CH_2-O), 51.7 (CH_2-N), 44.6 (CH_2-C≡), 41.5 (N-CH_3), 32.6 [CH_2-(CH_2O)], 30.3 (CH_2−Br), 29.8 (N-CH_3); MS (EI) *m*/*z* (%): 131 (60), 160 (100) [M − ((Br(CH_2)$_3$)-$CH_3NCH_2C{\equiv}CH$)]$^+$, 227 (7) [M − (Br(CH_2)$_3$)]$^+$, 281 (96) [$CH_3NCH_2C{\equiv}CH$)]$^+$, 348 (21)[M]$^+$. Anal. Calcd for $C_{17}H_{21}BrN_2O$: C, 58.46; H, 6.06; Br, 22.88; N, 8.02. Found: C, 58.49; H, 6.08; Br, 22.11; N, 8.23.

***N*-{[5-(3-(4-Benzylpiperidin-1-yl)propoxy)-1-methyl-1*H*-indol-2-yl]methyl}-*N*-methylprop-2-yn-1-amine (8).** 4-Benzylpiperidine (0.111 mL, 0.632 mmol, 2 equiv) was added to a mixture of **26** (111 mg, 0.316 mmol, 1 equiv) and potassium carbonate (131 mg, 0.648 mmol, 3 equiv) in *N*,*N*-dimethylformamide (4 mL). The reaction mixture was heated at 70 °C for 7 h under an atmosphere of argon. The reaction mixture was poured into water (5 mL) and extracted into dichloromethane (3 × 20 mL). The organic layers were combined, dried (Na_2SO_4), and concentrated. The residue was purified by column chromatography, eluting with 4% methanol in dichloromethane, affording compound **8** (89.2 mg, 64%) as white crystalline solid: R_f = 0.43 (CH_2Cl_2/MeOH, 10:1); mp 82−3 °C; IR (KBr) ν 3274, 2923, 1619, 1487, 1469, 1390, 1205, 1133, 1027 cm^{-1}; ^{1}H NMR (400 MHz, $CDCl_3$) δ 7.31−7.25 (m, 2H), 7.21−7.12 (m, 4H), 7.02 (d, *J* = 2.26 Hz, 1H, CH4-indole), 6.83 (dd, *J* = 8.83 and 2.43 Hz, 1H, CH6-indole), 6.32 (s, 1H, CH3-indole), 4.03 (t, *J* = 6.28 Hz, 2H, -CH_2O), 3.73 (s, 3H, CH_3), 3.67 (s, 2H, CH_2-N), 3.30 (d, *J* = 2.36 Hz, 2H, CH_2≡), 3.02 (d, *J* = 11.45 Hz, CH_2), 2.59 (t, *J* = 7.37 Hz, CH_2), 2.55 (d, *J* = 6.77 Hz, CH_2), 2.34 (s, 3H, CH_3), 2.29 (t, *J* = 2.33 Hz, C≡CH), 2.08−1.92 (m, 4H, 2 × CH_2), 1.66 (d, *J* = 12.7 Hz, CH_2), 1.55 (m, CH), 1.40 (qd, *J* = 12.19, 3.24 Hz, CH_2); ^{13}C NMR (100 MHz, $CDCl_3$) δ 153.1 (C5-indole), 140.5 (C-Ph), 137.0 (C2-indole), 133.3 (C7a-indole), 129.0 (2 × CH-Ph), 128.1 (2 × CH-Ph), 127.4 (C3a-indole), 125.7 (CH-Ph), 111.9 (CH6-indole), 109.5 (CH7-indole), 103.4 (CH4-indole), 102.0 (CH3-indole), 78.3 (≡CH), 73.4 (-C≡), 67.2 (CH_2-O), 55.7 (CH_2), 53.8 (2 × CH_2), 51.7 (CH_2), 44.7 (CH_2), 43.0 (CH_2), 41.5 (N-CH_3), 37.7 (CH), 31.7 (2 × CH_2), 29.8 (CH_3), 26.7 (CH_2); MS (ES) *m*/*z* (%) 188 (99), 444 (100) [M + H]$^+$, 445 (40) [M + 2H]$^+$, 466 (2)[M + Na]$^+$. Anal. Calcd for $C_{29}H_{37}N_3O$: C, 78.51; H, 8.41; N, 9.47. Found: C, 78.63; H, 8.59; N, 9.44. **8**·2HCl: white powder; mp 216−218 °C; IR (KBr) ν 3196, 2931, 2559, 2509, 1619, 1485, 1472, 1454, 1250, 1211 cm^{-1}; ^{1}H NMR (300 MHz, D_2O) δ 7.27 (d, *J* = 9.1 Hz, 1H, CH7-indole), 7.20−7.15 (m, 2H), 7.10−7.06 (m, 4H), 6.84 (dd, *J* = 9.0, 1.5 Hz, 1H, CH6-indole), 6.60 (s, 1H, CH3-indole), 4.48 (s, 2H, CH_2), 3.99 (t, *J* = 5.4 Hz, 2H, -CH_2O), 3.87 (s, 2H, CH_2), 3.59 (s, 3H, CH_3), 3.41 (d, *J* = 11.8 Hz, 2H, CH_2), 3.16−3.05 (m, 2H), 2.99−2.97 (m,1H, C≡CH), 2.81−267 (m, 5H, CH_2 + N-CH_3), 2.43 (d, *J* = 6.1 Hz, 2H, CH_2), 2.06−1.97 (m, 2H, CH_2), 1.74−1.70 (m, 3H, CH + CH_2), 1.34−1.22 (m, 2H, CH_2). Anal. Calcd for $C_{29}H_{37}N_3O\cdot2HCl\cdot{}^1/_2(H_2O)$: C, 66.27; H, 7.67; Cl, 13.49; N, 8.00. Found: C, 66.02; H, 7.62; Cl, 13.45; N, 8.25.

***N*-{[5-(3-(4-Benzylpiperazin-1-yl)propoxy)-1-methyl-1*H*-indol-2-yl]methyl}-*N*-methylprop-2-yn-1-amine (9).** 1-Benzylpiperazine (0.148 g, 0.845 mmol) was added to a mixture of **26** (0.147 g, 0.422 mmol) and potassium carbonate (0.116 g, 0.845 mmol) in *N*,*N*-dimethylformamide (10 mL). The reactants were heated at 70 °C overnight under an atmosphere of argon. The reaction mixture was poured into water (50 mL) and extracted into ethyl acetate (3 × 100 mL). The organic layers were combined, dried (Na_2SO_4), and concentrated in vacuo. The residue was purified by column chromatography, eluting with 2% MeOH in CH_2Cl_2, affording compound **9** (0.16 g, 85%) as a solid: R_f = 0.43 (CH_2Cl_2/MeOH, 10:1); mp 103−4 °C; IR (KBr) ν 3138, 2958, 2943, 2806, 2762, 1621, 1492, 1480, 1207, 1159 cm^{-1}; ^{1}H NMR (400 MHz, $CDCl_3$) δ 7.37−7.25 (m, 5H), 7.19 (d, *J* = 8.8 Hz, 1H, CH7-indole), 7.07 (d, *J* = 2.4 Hz, 1H, CH4-indole), 6.88 (dd, *J* = 8.8 and 2.4 Hz, 1H, CH6-indole), 6.35 (s, 1H, CH3-indole), 4.06 (t, *J* = 6.4 Hz, 2H, -CH_2O), 3.75 (s, 3H, N-CH_3), 3.69 (s, 2H, CH_2Ph), 3.54 (s, 2H, CH_2-N), 3.33 (d, *J* = 2.3 Hz, 2H, CH_2C≡), 2.53 (m, 8H, 4 × CH_2), 2.36 (s, 3H, N-CH_3), 2.32 (t, *J* = 2.3 Hz, 1H, C≡CH), 2.01 [m, 2H, CH_2(CH_2O)]; ^{13}C NMR (100 MHz, $CDCl_3$) δ 153.1 (C5-indole), 138.0 (C-Ph), 136.9 (C2-indole), 133.2 (C7a-indole), 129.1 (2 × CH-Ph), 128.1 (2 × CH-Ph), 127.4 (C3a-indole), 126.9 (CH-Ph), 111.9 (CH6-indole), 109.5 (CH7-indole), 103.2 (CH4-indole), 101.9 (CH3-indole), 78.3 (-C≡), 73.4 (≡CH), 67.1 (CH_2-O), 63.0 (CH_2-N), 55.33 (CH_2), 53.1 (CH_2), 53.0 (2 × CH_2), 51.7 (CH_2), 44.6 (CH_2), 41.5 (N-CH_3), 29.8 (N-CH_3), 26.9 [CH_2(CH_2O)]; MS (ES) *m*/*z* (%) 445 (100) [M + H]$^+$, 467 (2) [M + Na]$^+$. Anal. Calcd for $C_{28}H_{36}N_4O$: C, 75.64; H, 8.16; N, 12.60. Found: C, 75.39; H, 8.40; N, 12.52. **9**·3HCl: white powder; mp 227−230 °C; IR (KBr) ν 3195, 2953, 2561, 2516, 2442, 1620, 1485, 1472, 1442, 1211 cm^{-1}; ^{1}H NMR (300 MHz, D_2O) δ 7.36−7.31 (m, 5H), 7.27 (d, *J* = 9.1 Hz, 1H, CH7-indole), 7.05 (d, *J* = 2.4 Hz, 1H, CH4-indole), 6.84 (dd, *J* = 9.0, 2.5 Hz, 1H, CH6-indole), 6.61 (s, 1H, CH3-indole), 4.50 (s, 2H, CH_2), 4.21 (s, 2H, CH_2), 4.00 (t, *J* = 5.7 Hz, 2H, -CH_2O), 3.88 (d, *J* = 2.5 Hz, 2H, CH_2-C≡), 3.60 (s, 3H, CH_3), 3.50−3.35 (m, 4H), 3.33−3.22 (m, 2H), 2.98 (t, *J* = 2.5

Hz, 1H, C≡CH), 2.78 (s, 3H, N-CH_3), 2.14−1.98 (m, 2H, CH_2). Anal. Calcd for $C_{28}H_{39}Cl_3N_4O\cdot{}^1/_2(H_2O)$: C, 59.73; H, 7.16; N, 9.95. Found: C, 59.59; H, 7.49; N, 10.20.

Biological Evaluation. Inhibition Experiments of AChE and BuChE. To assess the inhibitory activity of the compounds toward AChE (EC 3.1.1.7) or BuChE (EC 3.1.1.8), we followed the spectrophotometric method of Ellman[78] using purified AChE from *Electrophorus electricus* (type V-S) or human recombinant (expressed in the HEK-293 cell line) or BuChE from equine or human serum (lyophilized powder) (Sigma-Aldrich, Madrid, Spain). The reaction took place in a final volume of 3 mL of a phosphate-buffered solution (0.1 M) at pH 8, containing 0.035 U/mL *Ee*AChE, 0.24 U/mL hrAChE, or 0.05 U/mL BuChE, and 0.35 mM 5,5′-dithiobis-2-nitrobenzoic acid (DTNB, Sigma-Aldrich, Madrid, Spain). Inhibition curves were made by preincubating this mixture with at least nine concentrations of each compound for 10 min. A sample with no compound was always present to determine the 100% of enzyme activity. After this preincubation period, acetylthiocholine iodide (0.35 mM) or butyrylthiocholine iodide (0.5 mM) (Sigma-Aldrich, Madrid, Spain) was added, allowing 15 min more of incubation, where the DTNB produces the yellow anion 5-thio-2-nitrobenzoic acid along with the enzymatic degradation of acetylthiocholine iodide or butyrylthiocholine iodide. Changes in absorbance were detected at 405 nm in a spectrophotometric plate reader (FluoStar OPTIMA, BMG Labtech). Compounds inhibiting AChE or BuChE activity would reduce the color generation; thus, IC_{50} values were calculated as the concentration of compound that produces 50% AChE activity inhibition. Data are expressed as the mean ± SEM of at least three different experiments in quadruplicate.

Kinetic Analysis of AChE Inhibition. To obtain estimates of the mechanism of action of compound **5**, reciprocal plots of $1/V$ versus $1/[S]$ were constructed at different concentrations of the substrate acetylthiocholine (0.1−1 mM) by using Ellman's method.[78] Experiments were performed in a transparent 48-well plate, each well containing 350 μL of the DTNB solution in PBS and 1 μL of buffer (control) or inhibitor solution to give the desired final concentration. Final volume (1 mL) was reached by adding phosphate buffer solution (pH 8). Reaction was initiated by adding 45 μL of AChE at 30 °C to give a final concentration of 0.18 U/mL. Progress curves were monitored at 412 nm over 1.33 min in a fluorescence plate reader Fluostar Optima (BMG-Technologies, Germany). Progress curves were characterized by a linear steady-state turnover of the substrate, and values of a linear regression were fitted according to Lineweaver−Burk replots using Origin software. The plots were assessed by a weighted least-squares analysis. Determination of Michaelis constant for the substrate ATCh was done at seven different concentrations (0.1−1 mM) to give K_M = 0.29 ± 0.01 mM and V_{max} = 2.82 ± 0.06 min^{-1}. Slopes of the reciprocal plots were then plotted against the concentration of **5** (0−10 μM) as previously described[80] to evaluate K_i data. Data analysis was performed with Origin Pro 7.5 software (Origin Lab Corp.).

Inhibition Experiments of MAO-A and MAO-B. A purification of mitochondria from rat liver homogenates was prepared as previously described[81] and used as source for MAO activities. Total protein was measured by the method of Bradford using bovine-serum albumin as standard. The inhibitory activity of the compounds toward MAO-A and MAO-B was determined following the method of Fowler and Tipton[82] using ^{14}C-labeled substrates (Perkinelmer, USA). MAO-B activity was determined toward 20 μM [^{14}C]phenylethylamine (PEA) (2.5 mCi/mmol) and MAO-A activity toward 100 μM [^{14}C]-(5-hydroxy-triptamine) (5-HT) (0.5 mCi/mmol). Inhibition curves were made by preincubating this mixture with at least nine concentrations of each compound for 30 min. A sample without compound was always present to determine the 100% of enzyme activity. The reaction was carried out at 37 °C in a final volume of 225 μL in 50 mM phosphate buffer (pH 7.2) and stopped by the addition of 100 μL of 2 M citric acid. Radiolabeled aldehyde product was extracted into toluene/ethyl acetate (1:1, v/v) containing 0.6% (w/v) 2, 5-diphenyloxazole (PPO) before liquid scintillation counting (Tri-Carb 2810TR). Data are the mean ± SEM of at least four different experiments in triplicate.

Reversibility Studies. To study the nature of the enzymatic inhibition exerted by **5**, we determined the activity of the enzyme in the presence and in the absence of the inhibitor by two different methods: after three consecutive washings with buffer and after different times of preincubation of the enzyme with the inhibitor. For the first method, enzyme samples were preincubated for 30 min at 37 °C with 6 nM compound **5** for MAO-A and 45 nM for MAO-B. Samples were then washed and centrifuged at 25000*g* for 10 min at 4 °C consecutively three times. Finally, total protein was measured and MAO-A and MAO-B activities were determined as above-described. For the second method, samples of enzyme and inhibitor **5** at the indicated concentration were preincubated for 0, 5, 15, and 30 min before measuring MAO-A and MAO-B activities as above-described.

Progress Curves of Substrate Consumption. To clarify the behavior of **5** toward MAO-A and MAO-B, the inhibitor was preincubated for long periods (0−420 min) with MAO-A (10 nM inhibitor concentration) and MAO-B (100 nM inhibitor concentration). The concentrations of **5** used in this assay were 2 times the corresponding IC_{50} value. After the corresponding periods, substrates were added and MAO activities were determined as above-described. Data are the mean ± SEM of three independent esperiments in triplicate.

Kinetic Analysis of MAO-B Inhibition. To obtain estimates of the mechanism of action of compound **5**, reciprocal plots of $1/V$ versus $1/[S]$ were constructed at different concentrations of the substrate β-phenylethylamine (1−200 μM) by using Fowler and Tipton's method.[82] The plots were assessed by a weighted least-squares analysis. Data analysis was performed with GraphPad Prism 3.0 software (GraphPad Software Inc.). Determination of Michaelis constants gave K_M = 6.7 ± 0.3 μM and V_{max} = 277.8 ± 6.1 pmol/min. Slopes of the reciprocal plots were then plotted against the concentration of **5** (0−10 μM) as previously described[79] to evaluate K_i data.

Inhibitory Capacity on $A\beta_{1-42}$ Self-Aggregation. The inhibition of $A\beta_{1-42}$ self-aggregation by compound **5** was studied by using the thioflavin T-based fluorometric assay previously described by Bartolini et al.[83] with little modifications. Briefly, $A\beta_{1-42}$ peptide (Bachem AG, Switzerland) was pretreatted with 1,1,1,3,3,3-hexafloro-2-propanol (HFIP, Sigma Chemicals) and redissolved in 10 mM phosphate buffer (PBS, pH 11.2 adjusted with NH_4OH). Final $A\beta_{1-42}$ stock solution concentration was 443 μM. To study the effect of **5** on fibril formation, experiments were performed by incubating the peptide (final Aβ concentration of 40 μM) with and without 10 μM compound **5** (Aβ/inhibitor = 4/1). Blanks containing only the inhibitor were also prepared. Propidium iodide (PI, Sigma-Aldrich) was used as reference compound in the experiments at the conditions described aboved and also at equimolar ratio Aβ/PI. Samples were diluted to a final volume of 200 μL with 10 mM PBS (pH 7.4), and 35 μM thioflavin T in 50 mM glycine−NaOH buffer (pH 8.5) was added. Experiments were performed on a Synergy HT microplate spectrofluorometer (Bio-Tek, U.S.). The fluorescence intensity was carried out (λ_{exc} = 485 nm; λ_{em} = 528 nm) every 10 min for 10 h, and values at plateau (400 min) were averaged after subtracting the background fluorescence of 35 μM thioflavin T solution. The fluorescence intensities were compared, and the percent inhibition due to the presence of the inhibitor was calculated by the following expression: $100 - [(IF_i/IF_0) \times 100]$, where IF_i and IF_0 are the fluorescence intensities obtained in the presence and absence of inhibitor, respectively.

Inhibition of hAChE-Induced $A\beta_{1-40}$ Aggregation. Aliquots of 231 μM $A\beta_{1-40}$ (Bachem AG, Switzerland) lyophilized from 1 mg/mL HFIP solution were redissolved in 10 mM phosphate buffer (PBS, pH 11.2 adjusted with NH_4OH). For co-incubation experiments, aliquots of human recombinant AChE (Sigma Chemicals) (0.4 μM final concentration, ratio Aβ/AChE = 10/1) in the presence of 100 μM compound **5** were added. Blanks containing Aβ, AChE, Aβ plus compound **5**, and AChE plus compound **5** were also prepared. To quantify the amyloid fibril formation, the thioflavin T fluorescence

method[82] was performed as above-described. The fluorescence intensities were compared, and the percent inhibition due to the presence of the inhibitor was calculated by the following expression: $100 - [(IF_i/IF_0) \times 100]$ where IF_i and IF_0 are the fluorescence intensities obtained in the presence and absence of inhibitor, respectively.

Molecular Modeling. Setup of the Systems. All protein models were derived from X-ray crystallographic structures taken from the Protein Data Bank (PDB). AChE models were built up from the AChE–donepezil complex 1EVE.[59] The enzyme was modeled in its physiological active form with neutral His440 and deprotonated Glu327, which together with Ser200 forms the catalytic triad. The standard ionization state at neutral pH was considered for the rest of the ionizable residues with the exception of Asp392 and Glu443, which were neutral, and His471, which was protonated, according to previous studies.[84] Three disulfide bridges were defined between Cys residues 66–93, 254–265, 402–521, and histidine residues 398 and 440 were set up to represent the δ tautomer.[85] MAO models were built up using X-ray structures 2Z5X[67] and 2C65[86] for isoforms A and B, respectively. Structural waters were defined as those common to five different high-resolution X-ray crystallographic structures (PDB entries 2Z5X, 2Z5Y, 2V5Z, 2C70, 2VZ2).

Docking. The binding mode of compound **5** was explored by means of docking calculations carried out with rDock, which is an extension of the program RiboDock, using an empirical scoring function calibrated on the basis of protein–ligand complexes.[64,65] Docking computations were performed with a 2-fold purpose: (1) to explore suitable starting orientations of the inhibitor in the binding site of AChE, MAO-A, and MAO-B and (2) to examine the docking of compound **5** for the three main orientations adopted by the indole ring of Trp279 in the peripheral binding site in *Torpedo californica* AChE.[61] At this point, it is worth noting that the reliability of rDock has been assessed by docking a set of known dual binding site IAChEs, taking advantage of the X-ray crystallographic structures of their complexes with AChE.[60] The docking of **5** in AChE was then explored using the three structural models of the target AChE differing in the orientations of Trp279 (PDB entries 1EVE, 1Q83, and 2CKM). Structural water molecules that mediate relevant interactions between the benzylpiperidine moiety and the enzyme were retained in the target models. Similarly, five water molecules found in the binding site of MAO-A and MAO-B were retained in docking calculations. The docking volume was defined as the space covered by catalytic, mid-gorge, and peripheral sites in AChE and by the substrate and entrance cavities in MAO. Suitable restraints were introduced to position the benzylpiperidine moiety of **5** in AChE. Each compound was subjected to 100 docking runs. Whereas the protein was kept rigid, rDock accounts for the conformational flexibility of the ligand around rotatable bonds during docking calculations. The output docking modes were analyzed by visual inspection in conjunction with the docking scores.

The X-ray structure of the recombinant human BuChE (PDB entry 2PM8)[87] was used to explore the binding mode of **5** in this enzyme. Some graphical manipulation was required, including addition of the hydrogen atoms according to the parm99SB force field and modeling of poorly resolved loop between residues Leu478 and Lys486, which was modeled using the X-ray structure of the BChE–tabun complex (PDB entry 3DJY).[88] Additionally, three disulfide bonds were defined between residues 94–120, 280–291, and 428–547. Residue Glu469 was modeled in the protonated state, and residue His466 was modeled as the Nδ-H tautomer. Docking calculations were performed using the same protocol mentioned above.

MM-PBSA Analysis. The ligand–protein poses were clusterized and reranked using the MM-PBSA approach in conjunction with the parmm99 force field of the AMBER (version 9) package.[89] The partial atomic charges of compound **5** were derived using the RESP protocol[90] by fitting to the molecular electrostatic potential calculated at the HF/6-31G* level with Gaussian 03.[91] Calculations were performed for 100 snapshots taken evenly during the last 5 ns of the simulations. The internal conformational energy was determined using the standard formalism and parameters implemented in AMBER. The electrostatic contribution was computed using a dielectric constant of 78.4 for the aqueous environment, while a dielectric constant of 1 was assigned to the interior of the protein. Even though the choice of the internal dielectric constant is a subject of debate, this value is usually adopted when calculations are performed for ensembles of snapshots taken from simulations, whereas higher values are generally used for calculations of static structures.[92,93] The electrostatic potentials were calculated using a grid spacing of 0.25 Å. Besides the standard atomic radii implemented in AMBER, calculations were also performed using a set of optimized radii developed for MM/PBSA computations with the AMBER force field.[66] The nonpolar contribution was calculated using a linear dependence with the solvent-accessible surface as implemented in AMBER. Finally, entropy changes upon complexation were assumed to cancel out in the comparison of the different poses.

Molecular Dynamics. The binding mode of compound **5** was explored by means of 20 ns molecular dynamics (MD) simulations performed for their complexes to AChE (using three different models; see above), MAO-A, and MAO-B. An additional MD simulation was run for the complex with donepezil and used to calibrate the results of the simulations performed for AChE complexes. In addition, MD simulations were also performed for the complexes corresponding to the covalent adduct formed between **5** and FAD in both MAO-A and MAO-B. To this end, suitable parameters were developed for the corresponding imine fragment formed in the chemical reaction (parameters available upon request to the authors).

The simulation protocol was based on the computational strategy used in our previous studies,[60] which is briefly summarized here. MD simulations were run using the PMEMD module of AMBER 9 and the parm99SB parameters for the protein.[94] The GAFF force field[95,96] was used to assign parameters to the inhibitor (and to the FAD cofactor in MAO simulations). The charge distribution of the inhibitor was further refined based on the electrostatic charges determined from a fit to the "HF/6-31G(d)" electrostatic potential obtained with Gaussian 03[91] using the RESP procedure. Na^+ cations were added to neutralize the negative charge of the system with the XLEAP module of AMBER 9. The system was immersed in an octahedral box of TIP3P[97] water molecules, preserving the crystallographic waters inside the binding cavity. The final systems contained the protein–ligand complex, Na^+ cations, and around 17 000 water molecules, leading to simulations systems that comprise around 53 000 atoms.

The geometry of the system was minimized in four steps. First, the position of hydrogen atoms was optimized using 3000 steps of steepest descent algorithm. Then water molecules were refined through 2000 steps of steepest descent followed by 3000 steps of conjugate gradient. Next, the ligand, water molecules, and counterions were optimized with 2000 steps of steepest descent and 4000 steps of conjugate gradient, and finally the whole system was optimized with 3000 steps of steepest descent and 7000 steps of conjugate gradient. Thermalization of the system was performed in five steps of 25 ps, increasing the temperature from 100 to 298 K. Concomitantly, the residues that define the binding site were restrained during thermalization using a variable restraining force. Thus, a force constant of 25 kcal mol^{-1} $Å^{-2}$ was used in the first stage of the thermalization and was subsequently decreased by increments of 5 kcal mol^{-1} $Å^{-2}$ in the next stages. Then a series of 20 ns trajectories were run for the two compounds using a time step of 1 fs. In MAO simulations, an additional restraint force was used for the backbone of residues 487–492, which define the transmembrane segment at the C-terminus of the protein. SHAKE was used for those bonds containing hydrogen atoms, in conjunction with periodic boundary conditions at constant pressure (1 atm) and temperature (298 K), particle mesh Ewald for the treatment of long-range electrostatic interactions, and a cutoff of 11 Å for nonbonded interactions.

■ ASSOCIATED CONTENT

Ⓢ Supporting Information

Representation of structural models derived from docking and MD simulations, as well as energetic analysis. This material is available free of charge via the Internet at http://pubs.acs.org.

AUTHOR INFORMATION

Corresponding Author

*For M.U.: phone, +34-93-5811439; fax, +34-93-5811573; e-mail, mercedes.unzeta@uab.es. For J.M.-C.: phone, +34-91-5622900; fax, +34-91-5644853; e-mail, iqoc21@iqog.csic.es.

Author Contributions

⊥These authors have contributed equally to this work.

ACKNOWLEDGMENTS

We thank the Ministerio de Ciencia e Innovación (Grants SAF2006-08764-C02-01, SAF2009-07271, and SAF2008-05595), Generalitat de Catalunya (2009-SGR00298), Comunidad de Madrid (Grant S/SAL-0275-2006), Instituto de Salud Carlos III [Retic RENEVAS (Grant RD06/0026/1002), Fundacion CIEN, Miguel Servet Program (Grant CP10/00531)], and COST Action D34/0003/05 (2005−2010) for financial support and the Centro de Supercomputació de Catalunya (CESCA) for computational facilities. A.S. and M.C. thank CSIC and Instituto de Salud Carlos III for postdoctoral I3P and "Sara Borrell" contracts, respectively. C.d.l.R. thanks MICINN for a Juan de la Cierva contract (2006−2008) and Instituto de Salud Carlos III for a Miguel Servet contract (2011−2016). J.J.-J. thanks Instituto de Salud Carlos III for PFIS fellowship FI10/00292. J.M.-C. thanks Prof. A. G. García (Departamento de Farmacología y Terapéutica, Facultad de Medicina, Universidad Autónoma de Madrid, Spain) for his interest and support. This work was realized in the framework of COST working group: D34/0003/05.

ABBREVIATIONS USED

AD, Alzheimer's disease; ACh, acetylcholine; AChE, acetylcholinesterase; Aβ, β-amyloid peptide; BuChE, butyrylcholinesterase; AChEI, acetylcholinesterase inhibitor; hAChE, human acetylcholinesterase; Ee, *Electrophorus electricus*; CAS, catalytic active site; PAS, peripheral anionic site; MAO, monoamine oxidase A/B; IMAO, monoamine oxidase inhibitor

REFERENCES

(1) Goedert, M.; Spillantini, M. G. A Century of Alzheimer's Disease. *Science* **2006**, *314*, 777−781.

(2) Terry, R. D.; Gonatas, N. K; Weiss, M. Ultrastructural Studies in Alzheimer's Presenile Dementia. *Ann. J. Pathol.* **1964**, *44*, 269−297.

(3) Grundke-Iqbal, I.; Iqbal, K.; Tung, Y. C.; Quinlan, M.; Wisniewski, H. M; Binder, L. I. Abnormal Phosphorylation of the Microtubule-Associated Protein τ (Tau) in Alzheimer Cystoskeletal Pathology. *Proc. Natl. Acad. Sci U.S.A.* **1986**, *93*, 4913−4917.

(4) Coyle, J. T; Puttfarcken, P. Oxidative Stress, Glutamate and Neurodegenerative Disorders. *Science* **1993**, *262*, 689−695.

(5) Gella, A.; Durany, N. Oxidative Stress in Alzheimer Disease. *Cell Adhes. Migr.* **2009**, *3*, 88−93.

(6) Perry, E. K.; Tomlinson, B. E.; Blesseed, G.; Bergmann, K.; Gibson, P. H.; Perry, R. H. Correlation of Cholinergic Abnormalities with Senile Plaques and Mental Test Scores in Senile Dementia. *Br. Med. J.* **1978**, *2*, 1457−1459.

(7) Talesa, V. N. Acetylcholinesterase in Alzheimer's Disease. *Mech. Ageing Dev.* **2001**, *122*, 1961−1969.

(8) García-Alloza, M.; Gil-Bea, F. J.; Díez-Ariza, M.; Chen, C. P.; Francis, P. T.; Lasheras, B.; Ramirez, M. J. Cholinergic−Serotonergic Imbalance Contributes to Cognitive and Behavioral Symptoms in Alzheimer's Disease. *Neurophsychologia* **2005**, *43*, 442−449.

(9) Terry, A. V.; Buccafusco, J. J.; Wilson, C. Cognitive Dysfunction in Neuropsychiatric Disorders: Selected Serotonin Receptor Subtypes as Therapeutic Targets. *Behav. Brain Res.* **2008**, *195*, 30−38.

(10) Dringenberg, H. C. Alzheimer's Disease: More Than a "Cholinergic Disorder": Evidence That Cholinergic−Monominergic Interactions Contribute to EEG Slowing and Dementia. *Behav. Brain Res.* **2000**, *115*, 235−249.

(11) Riederer, P.; Danielczyk, W.; Grünblatt, E. Monoamine Oxidase-B Inhibition in Alzheimer's Disease. *Neurotoxicology* **2004**, *25*, 271−277.

(12) Youdim, M. B.; Edmonson, D.; Tipton, K F. The Therapeutic Potential of Monoamine Oxidase Inhibitors. *Nat. Rev. Neurosci.* **2006**, *7*, 295−309.

(13) Youdim, M. B. H.; Finberg, J. P. M.; Tipton, K. F. Monoamine Oxidase. In *Handbook of Experimental Pharmacology*; Tredelenburg, U., Weiner, N., Eds.; Springer-Verlag: Berlin, 1988; Vol. *90*, pp 119−192.

(14) Johnston, J. P. Some Observations upon a New Inhibitor of Monoamine Oxidase in Brain Tissue. *Biochem. Pharmacol.* **1968**, *17*, 1285−1297.

(15) Grimsby, J.; Lan, N. C.; Neve, R.; Chen, K.; Shih, J. C. Tissue Distribution of Human Monoamine Oxidase A and B mRNA. *J. Neurochem.* **1990**, *55*, 1166−1169.

(16) Riederer, P.; Youdim, M. B. Monoamine Oxidase Activity and Monoamine Metabolism in the Brains of Parkinsonian Patients Treated with l-Deprenyl. *J. Neurochem.* **1986**, *46*, 1359−1365.

(17) Kristal, B. S.; Conway, A. D.; Brown, A. M.; Jain, J. C.; Ulluci, P. A.; Li, S. W.; Burke, J. W. Selective Dopaminergic Vulnerability: 3,4-Dihydroxyphenylacetaldehyde Targets Mitochondria. *Free Radical Biol. Med.* **2001**, *30*, 924−931.

(18) Pizzinat, N.; Copin, N.; Vindis, C.; Parini, A.; Cambon, C. Reactive Oxygen Species Production by Monoamineoxidases in Intact Cells. *Naunyn Schmiedeberg's Arch. Pharmacol.* **1999**, *359*, 428−431.

(19) Caraci, F.; Copani, A.; Nicoletti, F.; Drago, F. Depression and Alzheimer's Disease: Neurobiological Links and Common Pharmacological Targets. *Eur. J. Pharmacol.* **2010**, *626*, 64−71.

(20) Birks, J.; Harvey, R. Donepezil for Dementia Due to Alzheimer's Disease. *Cochrane Database Syst. Rev.* **2006**, No. 1, CD001190.

(21) Loy, C.; Schneider, L. Galantamine for Alzheimer's Disease. *Cochrane Database Syst. Rev.* **2004**, No. 4, CD001747.

(22) Birks, J.; Grimley, E. J.; Iakovidou, V. Rivastigmine for Alzheimer's Disease. *Cochrane Database Syst. Rev.* **2000**, No. 4, CD001191.

(23) Racchi, M.; Mazzucchelli, M.; Porrello, E.; Lanni, C.; Govoni, S. Acetylcholinesterase Inhibitors: Novel Activities of Old Molecules. *Pharmacol. Res.* **2004**, *50*, 441−451.

(24) Muñoz-Torrero, D. Acetylcholinesterase Inhibitors as Disease-Modifying Therapies for Alzheimer's Disease. *Curr. Med. Chem.* **2008**, *15*, 2433−2455.

(25) Castro, A.; Martínez, A. Targeting Beta-Amyloid Pathogenesis through Acetylcholinesterase Inhibitors. *Curr. Pharm. Des.* **2006**, *12*, 4377−4387.

(26) Cavalli, A.; Bolognesi, M. L.; Minarini, A.; Rosini, M.; Tumiatti, V.; Recanatini, M.; Melchiorre, C. Multi-Target-Directed Ligands To Combat Neurodegenerative Diseases. *J. Med. Chem.* **2008**, *51*, 347−372.

(27) Youdim, M. B.; Buccafusco, J. J. Multifunctional Drugs for Various CNS Targets in the Treatment of Neurodegenerative Disorders. *Trends Pharmacol. Sci.* **2005**, *26*, 27−35.

(28) Rodríguez-Franco, M. I.; Fernández-Bachiller, M. I.; Pérez, C.; Castro, A.; Martínez, A. Design and Synthesis of *N*-Benzylpiperidine-Purine Derivatives as New Dual Inhibitors of Acetyl- and Butyrylcholinesterase. *Bioorg. Med. Chem.* **2005**, *13*, 6795−6802.

(29) Rosini, M.; Antonello, A.; Cavalli, A.; Bolognesi, M. L.; Minarini, A.; Marucci, G.; Poggesi, E.; Leonardi, A.; Melchiorre, C. Prazosin-Related Compounds. Effect of Transforming the Piperazinylquinazoline Moiety into an Aminomethyltetrahydroacridine System on the Affinity for alpha1-Adrenoreceptors. *J. Med. Chem.* **2003**, *46*, 4895−4903.

(30) Elsinghorst, P. W.; Cieslik, J. S.; Mohr, K.; Tränkle, C.; Gütschow, M. The First Gallamine−Tacrine Hybrid: Design and Characterization at Cholinesterases and the M_2 Muscarinic Receptor. *J. Med. Chem.* **2007**, *50*, 5685−5695.

(31) Fang, L.; Appenroth, D.; Decker, M.; Kiehntopf, M.; Roegler, C.; Deufel, T.; Fleck, C.; Peng, S.; Zhang, Y.; Lehmann, J. Synthesis and Biological Evaluation of NO-Donor-Tacrine Hybrids as Hepatoprotective Anti-Alzheimer Drug Candidates. *J. Med. Chem.* **2008**, *51*, 713−716.
(32) Marco-Conelles, J.; León, R.; de los Ríos, C.; Guglietta, A.; Terencio, J.; López, M. G.; García, A. G.; Villarroya, M. Novel Multipotent Tacrine−Dihydropyridine Hybrids with Improved Acetylcholinesterase Inhibitory and Neuroprotective. Activities as Potential Drugs for the Treatment of Alzheimer's Disease. *J. Med. Chem.* **2006**, *49*, 7607−7610.
(33) Zheng, H.; Youdim, M. B. H.; Fridkin, M. Site-Activated Multifunctional Chelator with Acetylcholinesterase and Neuroprotective−Neurorestorative Moieties for Alzheimer's Therapy. *J. Med. Chem.* **2009**, *52*, 4095−4098.
(34) Sterling, J.; Herzig, Y.; Goren, T.; Finkelstein, N.; Lerner, D.; Goldenberg, W.; Mikcolczi, I.; Molnar, S.; Rantal, F.; Tamas, T.; Toth, G.; Zagyva, A.; Zekany, A.; Finberg, J.; Lavian, G.; Gross, A.; Friedman, R.; Razin, M.; Huang, W.; Krais, B.; Chorev, M.; Youdim, M. B.; Weinstock, M. Novel Dual Inhibitors of AChE and MAO Derived from Hydroxyl Aminoindan and Phenethylamine as Potential Treatment for Alzheimer's Disease. *J. Med. Chem.* **2002**, *54*, 5260−5279.
(35) Yogev-Falach, M.; Bar-Am, O.; Amit, T.; Weinreb, O.; Youdim, M. B. A Multifunctional, Neuroprotective Drug, Ladostigil (TV3326), Regulates Holo-APP Translation and Processing. *FASEB J.* **2006**, *20*, 2177−2179.
(36) Youdim, M. B.; Weinstock, M. Molecular Basis of Neuroprotective Activities of Rasagiline and the Anti-Alzheimer Drug TV3326, [(*N*-Propargyl-(3*R*)Aminoindan-5-yL)-ethyl methyl carbamate]. *Cell. Mol. Neurobiol.* **2002**, *21*, 555−573.
(37) Youdim, M. B.; Amit, T.; Bar-Am, O.; Weinreb, O.; Yogev-Falach, M. Implications of Co-Morbidity for Etiology and Treatment of Neurodegenerative Diseases with Multifunctional, Neuroprotective−Neurorescue Drugs; Ladostigil. *Neurotoxic. Res.* **2006**, *10*, 181−192.
(38) Bar-Am, O.; Amit, T.; Weinreb, O.; Youdim, M. B.; Mandel, S. Propargylamine-Containing Compounds as Modulators of Proteolitic Cleavage of Amyloid-Beta Protein Precursor: Involvement of MAPK and PKC Activation. *J. Alzheimer's Dis.* **2010**, *21*, 361−371.
(39) Elsinghorst, P. W.; Härtig, W.; Goldhammer, S.; Grosche, J.; Gütschow, M. A Gorge-Spanning, High Affinity, Cholinesterase Inhibitor to Explore Beta-Amyloid Plaques. *Org. Biomol. Chem.* **2009**, *7*, 3940−3946.
(40) Zheng, H.; Youdim, M. B.; Fridkin, M. Site-Activated Chelators Targeting Acetylcholinesterase and Monoamine Oxidase for Alzheimer's Therapy. *ACS Chem. Biol.* **2010**, *5*, 603−610.
(41) Palermo, M.; Bores, G.; Huger, F.; Kurys, B.; Merriman, M.; Olsen, G.; Ong, H.; Petko, W.; O'Malley, G. Combined AChE and Reversible MAO Inhibition as a Potential Therapeutic Approach for Senile Dementia of the Alzheimer Type. *Abstracts of Papers*, 205th National Meeting of the American Chemical Society, 1993; American Chemical Society: Washington DC, 1993.
(42) Fink, D. M.; Palermo, M. G.; Bores, G. M.; Huger, F.; Kurys, B.; Merriman, M.; Olsen, G.; Ong, H.; Petko, W.; O'Malley, G. Imino 1,2,3,4-Tetrahydrocyclopent[*b*]-indole Carbamates as Dual Inhibitors of Acetylcholinesterase and Monoamine Oxidase. *Bioorg. Med. Chem. Lett.* **1996**, *6*, 625−630.
(43) Bruhlmann, C.; Ooms, F.; Carrupt, P. A.; Testa, B.; Catto, M.; Leonetti, F.; Altomare, C.; Carotti, A. Coumarins Derivatives as Dual Inhibitors of Acetylcholinesterase and Monoamine Oxidase. *J. Med. Chem.* **2001**, *44*, 3195−3198.
(44) Cruces, M. A.; Elorriaga, C.; Fernandez-Alvarez, E.; Nieto, O. Acetylenic and Allenic Derivatives of 2-(5-Methoxyindolyl)methylamine Synthesis and Evaluation as Selective Inhibitors of Monoamine Oxidases A and B. *Eur. J. Med. Chem.* **1990**, *25*, 257−265.
(45) Morón, J. A.; Campillo, M.; Pérez, V.; Unzeta, M.; Pardo, L. Molecular Determinants of MAO Selectivity in a Series of Indolylmethylamine Derivatives: Biological Activities, 3D-QSAR/CoMFA Analysis, and Computational Simulation of Ligand Recognition. *J. Med. Chem.* **2000**, *43*, 1684−1691.
(46) Pérez, V.; Marco, J. L.; Fernández-Álvarez, E.; Unzeta, M. Relevance of Benzyloxy Group in 2-Indolyl Methylamines in the Selective MAO-B Inhibition. *Br. J. Pharmacol.* **1999**, *127*, 869−876.
(47) Inestrosa, N. C.; Alvarez, A.; Pérez, C. A.; Moreno, R. D.; Vicente, M.; Linker, C.; Casanueva, O. I.; Soto, C.; Garrido, J. Acetylcholinestearse Accelerates Assembly of Amyloid-Beta-Peptides into Alzheimer's Fibrils: Possible Role of the Peripheral Site of the Enzyme. *Neuron* **1996**, *16*, 881−891.
(48) De Ferrari, G. V.; Canales, M. A.; Shin, I.; Weiner, L. M.; Silman, I.; Inestrosa, N. C. A Structural Motif of Acetylcholinesterase That Promotes Amyloid Beta-Peptide Fibril Formation. *Biochemistry* **2001**, *40*, 10447−10457.
(49) Rees, T. M.; Berson, A.; Sklan, E. H.; Younkin, L.; Younkin, S.; Brimijoin, S.; Soreq, H. Memory Deficits Correlating with Acetylcholinesterase Splice Shift and Amyloid Burden in Doubly Transgenic Mice. *Curr. Alzheimer Res.* **2005**, *2*, 291−300.
(50) Dinamarca, M. C.; Sagal, J. P.; Quintanilla, R. A.; Godoy, J. A.; Arrázola, M. S.; Inestrosa, N. C. Amyloid-beta-Acetylcholinesterase Complexes Potentiate Neurodegenerative Changes Induced by the Abeta Peptide. Implications for the Pathogenesis of Alzheimer's Disease. *Mol. Neurodegener.* **2010**, *5*, 4.
(51) Cruces, M. A.; Elorriaga, C.; Fernández-Álvarez, E. The Kinetics of Monoamine Oxidase Inhibition by Three 2-Indolylmethylamine Derivatives. *Biochem. Pharmacol.* **1990**, *40*, 535−543.
(52) Contreras, J. M.; Parrot, I.; Sippl, W.; Rival, Y. M.; Wermuth, C. G. Design, Synthesis, and Structure−Activity Relationships of a Series of 3-[2-(1-Benzylpiperidin-4-yl)ethylamino]pyridazine Derivatives as Acetylcholinesterase Inhibitors. *J. Med. Chem.* **2001**, *44*, 2707−2718.
(53) Hallinan, E. A.; Hagen, T. J.; Husa, R. K.; Tsymbalov, S.; Rao, S. N.; van Hoeck, J. P.; Rafferty, M. F.; Stapelfeld, A.; Savage, M. A.; Reichman, M. N. Substituted Dibenzoxazepines as Analgesic PGE2 Antagonists. *J. Med. Chem.* **1993**, *36*, 3293−3299.
(54) Yamanaka, T.; Ohkubo, M.; Kuroda, S.; Nakamura, H.; Takahashi, F.; Aoki, T.; Mihara, K.; Seki, J.; Kato, M. Design, Synthesis, and Structure−Activity Relationships of Potent GPIIb/IIIa Antagonists: Discovery of FK419. *Bioorg. Med. Chem.* **2005**, *13*, 4343−4352.
(55) Frølund, B.; Kristiansen, U.; Brehm, L.; Hansen, A. B.; Krogsgaard-Larsen, P.; Falch, E. Partial GABAA Receptor Agonists. Synthesis and in Vitro Pharmacology of a Series of Nonannulated Analogs of 4,5,6,7-Tetrahydroisoxazolo[4,5-*c*]pyridin-3-ol. *J. Med. Chem.* **1995**, *38*, 3287−3296.
(56) Kitbunnadaj, R.; Zuiderveld, O. P.; De Esch, I. J. P.; Vollinga, R. C.; Bakker, R.; Lutz, M.; Spek, A. L.; Cavoy, E.; Deltent, M. F.; Menge, W. M. P. B.; Timmerman, H.; Leurs, R. Synthesis and Structure−Activity Relationships of Conformationally Constrained Histamine H_3 Receptor Agonists. *J. Med. Chem.* **2003**, *46*, 5445−5457.
(57) Mandelli, G. R.; Maiorana, S.; Terni, P.; Lamperti, G.; Colibretti, M. L.; Imbimbo, B. P. Synthesis of New Cardioselective M_2 Muscarinic Receptor Antagonists. *Chem. Pharm. Bull.* **2000**, *48*, 1611−1622.
(58) Greig, N. H.; Utsuki, T.; Ingram, D.; Wang, K. Y.; Pepeu, G.; Scali, C.; Yu, Q. S.; Mamczarz, J.; Holloway, H. W.; Giordano, T.; Chen, D.; Furukawa, K.; Sambamurti, K.; Brossi, A.; Lahiri, D. K. Selective Butyrylcholinesterase Inhibition Elevates Brain Acetylcholine, Augments Learning and Lowers Amyloid-β Peptide in Rodents. *Proc. Natl. Acad. Sci. U.S.A.* **2005**, *102*, 17213−17218.
(59) Kryger, G.; Silman, I.; Sussman, J. L. Structure of Acetylcholinesterase Complexed with E2020 (Aricept): Implications for the Design of New Anti-Alzheimer Drugs. *Structure* **1999**, *7*, 297−307.
(60) Camps, P.; Formosa, X.; Galdeano, C.; Muñoz-Torrero, D.; Ramírez, L.; Gómez, E.; Isambert, N.; Lavilla, R.; Badia, A.; Clos, M. V.; Bartolini, M.; Mancini, F.; Andrisano, V.; Arce, M. P.; Rodríguez-Franco, M. I.; Huertas, O.; Dafni, T.; Luque, F. J. Pyrano[3,2-*c*]quinoline-6-chlorotacrine Hybrids as a Novel Family of

Acetylcholinesterase- and Beta-Amyloid-Directed Anti-Alzheimer Compounds. *J. Med. Chem.* **2009**, *52*, 5365−5379.
(61) Galdeano, C.; Viayna, E.; Arroyo, P.; Bidon-Chanal, A.; Blas, J. R.; Muñoz-Torrero, D.; Luque, F. J. Structural Determinants of the Multifunctional Profile of Dual Binding Site Acetylcholinesterase Inhibitors as Anti-Alzheimer Agents. *Curr. Pharm. Des.* **2010**, *16*, 2818−2836.
(62) Rydberg, E. H.; Brumshtein, B.; Greenblatt, H. M.; Wong, D. M.; Shaya, D.; Williams, L. D.; Carlier, P. R.; Pang, Y.-P.; Silman, I.; Sussman, J. L. Complexes of Alkylene-Linked Tacrine Dimers with *Torpedo californica* Acetylcholinesterase: Binding of Bis(5)-tacrine Produces a Dramatic Rearrangement in the Active-Site Gorge. *J. Med. Chem.* **2006**, *49*, 5491−5500.
(63) Bourne, Y.; Kolb, H. C.; Radic, Z; Sharpless, K. B.; Taylor, P.; Marchot, P. Freeze-Frame Inhibitor Captures Acetylcholinesterase in a Unique Conformation. *Proc. Natl. Acad. Sci. U.S.A.* **2004**, *101*, 1449−1454.
(64) Morley, S. D.; Afshar, M. Validation of an Empirical RNA-Ligand Scoring Function for Fast Flexible Docking Using RiboDock. *J. Comput.-Aided Mol. Des.* **2004**, *18*, 189−208.
(65) Barril, X.; Hubbard, R. E.; Morley, S. D. Virtual Screening in Structure-Based Drug Discovery. *Mini-Rev. Med. Chem.* **2004**, *4*, 779−791.
(66) Swanson, J. M. J.; Adcock, S. A.; McCammon, J. A. Optimized Radii for Poisson−Boltzmann Calculations with the AMBER Force Field. *J. Chem. Theory Comput.* **2005**, *1*, 484−493.
(67) Son, S.-Y.; Ma, J.; Kondou, Y.; Yoshimura, M.; Yamashita, E.; Tsukihara, T. Structure of Human Monoamine Oxidase A at 2.2-Å Resolution: The Control of Opening the Entry for Substrates/Inhibitors. *Proc. Natl. Acad. Sci. U.S.A.* **2008**, *105*, 5739−5744.
(68) De Colibus, L.; Li, M.; Binda, C.; Lustig, A.; Edmondson, D. E.; Mattevi, A. Three-Dimensional Structure of Human Monoamino Oxidase A (MAO A): Relation to the Structures of Rat MAO A and Human MAO B. *Proc. Natl. Acad. Sci. U.S.A.* **2005**, *102*, 12684−12689.
(69) Binda, C.; Hubálek, F.; Li, M.; Herzig, Y.; Sterling, J.; Edmonson, D. E.; Mattevi, A. Crystal Structures of Monoamine Oxidase B in Complex with Four Inhibitors of the *N*-Propargylaminoindan Class. *J. Med. Chem.* **2004**, *47*, 1767−1774.
(70) Cavalli, A.; Bolognesi, M. L.; Capsoni, S.; Andrisano, V.; Bartolini, M.; Margotti, E.; Cattaneo, A.; Recanatini, M.; Melchiorre, C. A Small Molecule Targeting the Multifactorial Nature of Alzheimer's Disease. *Angew. Chem., Int. Ed.* **2007**, *46*, 3689−3692.
(71) Muñoz-Ruiz, P.; Rubio, L.; García-Palomero, E.; Dorronsoro, I.; del Monte-Millán, M.; Valenzuela, R.; Usán, P.; de Austria, C.; Bartolini, M.; Andrisano, V.; Bidon-Chanal, A.; Orozco, M.; Luque, F. J.; Medina, M.; Martínez, A. Design, Synthesis, and Biological Evaluation of Dual Binding Site Acetylcholinesterase Inhibitors: New Disease-Modifying Agents for Alzheimer's Disease. *J. Med. Chem.* **2005**, *48*, 7223−7233.
(72) Bolognesi, M. L.; Banzi, R.; Bartolini, M.; Cavalli, A.; Tarozzi, A.; Andrisano, V.; Minarini, A.; Rosini, M.; Tumiatti, V.; Bergamini, C.; Fato, R.; Lenaz, G.; Hrelia, P.; Cattaneo, A.; Recanatini, M.; Melchiorre, C. Novel Class of Quinone-Bearing Polyamines as Multi-Target-Directed Ligands To Combat Alzheimer's Disease. *J. Med. Chem.* **2007**, *50*, 4882−4897.
(73) Tumiatti, V.; Milelli, A.; Minarini, A.; Rosini, M.; Bolognesi, M. L.; Micco, M.; Andrisano, V.; Bartolini, M.; Mancini, F.; Recanatini, M.; Cavalli, A.; Melchiorre, C. Structure−Activity Relationships of Acetylcholinesterase Noncovalent Inhibitors Based on a Polyamine Backbone. 4. Further Investigation on the Inner Spacer. *J. Med. Chem.* **2008**, *51*, 7308−7312.
(74) Bolognesi, M. L.; Bartolini, M.; Rosini, M.; Andrisano, V.; Melchiorre, C. Structure−Activity Relationships of Memoquin: Influence of the Chain Chirality in the Multi-Target Mechanism of Action. *Bioorg. Med. Chem. Lett.* **2009**, *19*, 4312−4315.
(75) Zhou, Y.; Jiang, C.; Zhang, Y.; Liang, Z.; liu, W.; Wang, L.; Luo, C.; Zhong, T.; Sun, Y.; Zhao, L.; Xie, X.; Jiang, H.; Zhou, N.; Liu, D.; Liu, H. Structural Optimization and Biological Evaluation of Substituted Bisphenol A Derivatives as beta-Amyloid Peptide Aggregation Inhibitors. *J. Med. Chem.* **2010**, *53*, 5449−5466.
(76) Jacob-Roetne, R.; Jacobsen, H. Alzheimer's Disease: From Pathology to Therapeutic Approaches. *Angew. Chem., Int. Ed.* **2009**, *48*, 3030−3059.
(77) Perry, E. K.; Perry, R. H.; Blessed, G.; Tomlinson, B. E. Changes in Brain Cholinesterases in Senile Dementia of Alzheimer Type. *Neuropathol. Appl. Neurobiol.* **1978**, *4*, 273−277.
(78) Greig, N. H.; Utsuki, T.; Yu, Q.; Zhu, X.; Holloway, H. W.; Perry, T.; Lee, B.; Ingram, D. K.; Lahiri, K. A New Therapeutic Target in Alzheimer's Disease Treatment: Attention to Butyrylcholinesterase. *Curr. Med. Res. Opin.* **2001**, *17*, 159−165.
(79) Ellman, G. L.; Courtney, K. D.; Andres, V.; Featherstone, R. M. A New and Rapid Colorimetric Determination of Acetylcholinesterase Activity. *Biochem. Pharmacol.* **1961**, *7*, 88−95.
(80) Segel, I. H. *Enzyme Kinetics*; John Wiley: Toronto, Canada, 1975; p 838.
(81) Gomez, N.; Unzeta, M.; Tipton, K. F.; Anderson, M. C.; O'Carrol, A. M. Determination of Monoamino Oxidase Concentrations in Rat Liver by Inhibitor Binding. *Biochem. Pharmacol.* **1986**, *35*, 4467−4472.
(82) Fowler, C. J.; Tipton, K. F. Concentration Dependence of the Oxidation of Tyramine by the Two Forms of Rat Liver Mitochondrial Monoamine Oxidase. *Biochem. Pharmacol.* **1981**, *30*, 3329−3332.
(83) Bartolini, M.; Bertucci, C.; Cavrini, V.; Andrisano, V. Beta-Amyloid Aggregation Induced by Human Acetylcholinestrase: Inhibition Studies. *Biochem. Pharmacol.* **2003**, *65*, 407−416.
(84) Wlodek, S. T.; Antosiewicz, J.; McCammon, J. A.; Straatsma, T. P.; Gilson, M. K.; Briggs, J. M.; Humblet, C.; Sussman, J. L. Binding of Tacrine and 6-Chlorotacrine by Acetylcholinesterase. *Biopolymers* **1996**, *38*, 109−117.
(85) Dvir, H.; Wong, D. M.; Harel, M.; Barril, X.; Orozco, M.; Luque, F. J.; Muñoz-Torrero, D.; Camps, P.; Rosenberry, T. L.; Silman, I.; Sussman, J. L. 3D Structure of *Torpedo californica* Acetylcholinesterase Complexed with Huprine X at 2.1 Å Resolution: Kinetic and Molecular Dynamic Correlates. *Biochemistry* **2002**, *41*, 2970−2981.
(86) Binda, C.; Hubalek, F.; Li, M.; Herzig, Y.; Sterling, J.; Edmonson, D. E.; Mattevi, A. Binding of Rasagiline-Related Inhibitors to Human Monoamine Oxidases: A Kinetic and Crystallographic Analysis. *J. Med. Chem.* **2005**, *48*, 8148−8154.
(87) Ngamelue, M. N.; Homma, K.; Lockridge, O.; Asojo, O. A. Crystallization and X-ray Structure of Full-Length Recombinant Human Butytylcholinesterase. *Acta Crystallogr., Sect. F* **2007**, *63*, 723−727.
(88) Carletti, E.; Li, H.; Li, B.; Ekström, F.; Nicolet, Y.; Loiodice, M.; Gillon, E.; Froment, M. T.; Lockridge, O.; Schopfer, L. M.; Masson, P.; Nachon, F. Aging of Cholinesterases Phosphylated by Tabun Proceeds through O-Dealkylation. *J. Am. Chem. Soc.* **2008**, *130*, 16011−16020.
(89) Case, D. A.; Darden, T. A.; Cheatham, T. E., III; Simmerling, C. L.; Wang, J.; Duke, R. E.; Luo, R.; Merz, K. M.; Pearlman, D. A.; Crowley, M.; Walker, R. C.; Zhang, W.; Wang, B.; Hayik, S.; Roitberg, A.; Seabra, G.; Wong, K. F.; Paesani, F.; Wu, X.; Brozell, S.; Tsui, V.; Gohlke, H.; Yang, L.; Tan, C.; Mongan, J.; Hornak, V.; Cui, G.; Beroza, P.; Mathews, D. H.; Schafmeister, C.; Ross, W. S.; Kollman, P. A. *AMBER*, version 9; University of California: San Francisco, CA, 2006.
(90) Bayly, C. I.; Cieplak, P.; Cornell, W. D.; Kollman, P. A. *J. Phys. Chem.* **1993**, *97*, 10269−10280.
(91) Frisch, M. J.; Trucks, G. W.; Schlegel, H. B.; Scuseria, G. E.; Robb, M. A.; Cheeseman, J. R.; Montgomery, J. A., Jr.; Vreven,T.; Kudin, K. N.; Burant, J. C.; Millam, J. M.; Iyengar, S. S.; Tomasi, J.; Barone, V.; Mennucci, B.; Cossi, M.; Scalmani, G.;Rega, N.; Petersson, G. A.; Nakatsuji, H.; Hada, M.; Ehara, M.; Toyota, K.; Fukuda, R.; Hasegawa, J.; Ishida, M.; Nakajima, T.; Honda, Y.; Kitao, O.; Nakai, H.; Klene, M.; Li, X.; Knox, J. E.; Hratchian, H. P.; Cross, J. B.; Adamo, C.; Jaramillo, J.; Gomperts, R.; Stratmann, R. E.; Yazyev, O.; Austin, A. J.; Cammi, R.; Pomelli, C.; Ochterski, J. W.; Ayala, P. Y.; Morokuma, K.; Voth, G. A.; Salvador, P.; Dannenberg, J. J.; Zakrzewski, V. G.; Dapprich, S.; Daniels, A. D.; Strain, M. C.;

Farkas, O.; Malick, D. K.; Rabuck, A. D.; Raghavachari, K.; Foresman, J. B.; Ortiz, J. V.; Cui, Q.; Baboul, A. G.; Clifford, S.; Cioslowski, J.; Stefanov, B. B.; Liu, G.; Liashenko, A.; Piskorz, P.; Komaromi, I.; Martin, R. L.; Fox, D. J.; Keith, T.; Al-Laham, M. A.; Peng, C. Y.; Nanayakkara, A.; Challacombe, M.; Gill, P. M. W.; Johnson, B.; Chen, W.; Wong, M. W.; Gonzalez, C.; Pople, J. A. *Gaussian 03*, revision B.04, Gaussian, Inc.: Pittsburgh PA, 2003.

(92) Srinivasan, J.; Cheatham, T. E. III; Cieplak, P.; Kollman, P. A.; Case, D. A. Continuum Solvent Studies of the Stability of DNA, RNA and Phosphoramidate-DNA Helices. *J. Am. Chem. Soc.* **1998**, *120*, 9401−9409.

(93) Stoica, I.; Sadiq, S. K.; Coveney, P. V. Rapid and Accurate Prediction of Binding Free Energies for Saquinavir-Bound HIV-1 Proteases. *J. Am. Chem. Soc.* **2008**, *130*, 2639−2648.

(94) Homak, V.; Abel, R.; Okur, A.; Strockbine, B.; Roitberg, A.; Simmerling, C. Comparison of Multiple Amber Force Fields and Development of Improved Protein Backbone Parameters. *Proteins* **2006**, *65*, 712−725.

(95) Wang, J.; Wolf, R. M.; Caldwell, J. W.; Kollman, P. A.; Case, D. A. Development and Testing of a General AMBER Force Field. *J. Comput. Chem.* **2004**, *25*, 1157−1174.

(96) Wang, J.; Wang, W.; Kollman, P. A.; Case, D. A. Automatic Atom Type and Bond Type Perception in Molecular Mechanical Calculations. *J. Mol. Graphics Modell.* **2006**, *25*, 247−260.

(97) Jorgensen, W. L.; Chandrasekhar, J.; Madura, J. D.; Impey, R. W.; Klein, M. L. Comparison of Simple Potential Functions for Simulating Liquid Water. *J. Chem. Phys.* **1983**, *79*, 926−935.